



## Historical drought patterns over Canada and their relation to teleconnections

Zilefac Elvis Asong<sup>1</sup>, Howard Simon Wheeler<sup>1</sup>, Barrie Bonsal<sup>2</sup>, Saman Razavi<sup>1</sup>, Sopan Kurkute<sup>1</sup>

<sup>1</sup>*Global Institute for Water Security and School of Environment and Sustainability, University of Saskatchewan, 11 Innovation Blvd, Saskatoon, SK, Canada S7N 3H5*

<sup>2</sup>*Environment and Climate Change Canada, 11 Innovation Blvd, Saskatoon, SK, Canada S7N 3H5*

### Highlights

- 1) Two main spatially disjunctive sub-regions of drought variability over Canada are identified
- 2) Interannual periodicities dominate drought variability over the two sub-regions
- 3) These cycles of low-frequency variability are teleconnected principally to the PNA and MEI indices

### \*Corresponding author:

Phone: +1 306 491 9565

Email: [elvis.asong@usask.ca](mailto:elvis.asong@usask.ca)



## 26 Abstract

27 Drought is a recurring extreme climate event and among the most costly natural disasters in the world. This  
28 is particularly true over Canada, where drought is both a frequent and damaging phenomenon with impacts  
29 on regional water resources, agriculture, industry, aquatic ecosystems and health. However, nation-wide  
30 drought assessments are currently lacking and impacted by limited ground-based observations. This study  
31 provides a comprehensive analysis of historical droughts over the whole of Canada, including the role of  
32 large-scale teleconnections. Drought events are characterized by the Standardized Precipitation-  
33 Evapotranspiration Index (SPEI) over various temporal scales (1, 3, 6, and 12 consecutive months, 6 months  
34 from April to September, and 12 months from October to September) applied to different gridded monthly  
35 data sets for the period 1950 – 2013. The Mann Kendall test, Rotated Empirical Orthogonal Function,  
36 Continuous Wavelet Transform, and Wavelet Coherence analyses are used, respectively, to investigate the  
37 trend, spatiotemporal patterns, periodicity, and teleconnectivity of drought events. Results indicate that  
38 southern (northern) parts of the country experienced significant trends towards drier (wetter) conditions  
39 although substantial variability exists. Two spatially well-defined regions with different temporal evolution  
40 of droughts were identified—the Canadian Prairies and Northern-central Canada. The analyses also  
41 revealed the presence of a dominant periodicity of between 8 – 32 months in the Prairie region, and 8 – 40  
42 months in the Northern central region. These cycles of low-frequency variability are found to be associated  
43 principally to the Pacific-North American (PNA) and Multivariate El Niño/Southern Oscillation Index  
44 (MEI) relative to other considered large-scale climate indices. This study is the first of its kind to identify  
45 dominant periodicities in drought variability over the whole of Canada in terms of when the drought events  
46 occur, the duration, and how often they do so.

47 **Keywords:** Drought; SPEI; periodicity; teleconnections; ground-based observations, Canada

48

49



## 50    **1    Introduction**

51            Drought is a naturally occurring environmental phenomenon and a major natural hazard that can have  
52    devastating impacts on regional water resources, agriculture, industry and other social-ecological systems,  
53    with far-reaching impacts in an increasingly globalized and uncertain world (IPCC, 2013; Sternberg, 2011).  
54    Although still among the least understood extreme weather events affecting larger areas, droughts have  
55    proved to be the costliest and most widespread of natural disasters (Bryant, 2005; Wilhite, 2000a). This is  
56    primarily due to their usually lengthy duration, severity and large spatial extent, sometimes reaching  
57    continental scales and lasting for many years (Sheffield et al., 2009). Generally, droughts can affect all  
58    components of the hydrological cycle, from its origin as a deficit in precipitation— $P$  (Dai, 2011; Palmer,  
59    1965; McKee et al., 1993), to its combination with high evapotranspiration losses that can lead to a deficit  
60    in soil moisture and subsequent manifestation into a hydrological drought (Tallaksen and Stahl, 2014).

61            A review of key drought concepts (e.g. classification and indices) and the relation between droughts  
62    and large-scale climate indices has been carried out by Mishra and Singh (2010). However, due to the wide  
63    variety of sectors affected by droughts, their diverse spatial and temporal structures, the inter-dependence  
64    across climatic, hydrologic, geomorphic, ecological and societal variables, and the demand placed on water  
65    supply by different users, there is no universal definition of droughts and associated impacts. The most used  
66    drought classification is that initially proposed by Dracup et al. (1980) and later integrated by Wilhite and  
67    Glantz (1985) and Wilhite (2000b); Wilhite and Glantz (1985). Based on the degree of water deficit,  
68    droughts are often classified into three types including (1) meteorological, (2) agricultural, and (3)  
69    hydrological. Further details on drought classification and definitions are found in (Mishra and Singh,  
70    2010; Dai, 2011; Van Loon et al., 2016).

71            Studies on regional drought characteristics are important and should be incorporated in water  
72    resources management efforts (Mishra and Singh, 2011; Wheeler and Gober, 2013). Of particular interest  
73    is the analysis of drought occurrence over Canada, a country in which drought is among the most costly  
74    natural hazards, particularly in the interior Prairie region, e.g., Bonsal et al. (2011). During the period 1950–  
75    2010, nationwide annual mean surface air temperature— $T$  increased by 1.5°C (Vincent et al., 2012). Being



76 the second largest country in the world and with a large continental interior, this rapid warming has been  
77 accompanied by significant changes in many other hydroclimatic elements in different parts of the country,  
78 including increases in  $P$  (Mekis and Vincent, 2011), decreases in the duration of snow cover (Brown and  
79 Braaten, 1998), and decreases in annual streamflow (Zhang et al., 2001). Climate projections also indicate  
80 that many regions of Canada will likely experience increasing drought risk by the end of the 21<sup>st</sup> century  
81 (Masud et al., 2017; Bonsal et al., 2013; Dibike et al., 2017).

82 Historically, most areas of Canada have experienced periodic droughts with different durations,  
83 severities, and marked spatial extent, but the agricultural belt of the Canadian Prairies has tended to be  
84 highly susceptible to droughts due in part to its location in the lee of the Rocky Mountains and its strong  
85 dependence on rain-fed agriculture (Shabbar and Skinner, 2004). In particular, devastating drought events  
86 over western Canada during the 1890s, 1910s, 1930s, 1960s, 1980s, 1999 – 2005, and most recently in 2015  
87 have been identified by using a variety of drought indicators at various scales (Bonsal et al., 2011b; Bonsal  
88 and Regier, 2007; Szeto et al., 2016). The 1961 drought (the worst single year drought on the Prairies, with  
89 about 50% of normal growing season precipitation) led to a total net farm income drop of 48% (\$300  
90 million) compared with the previous year (Bonsal et al., 1999). The drought of 1988 had many impacts on  
91 the agricultural sectors of Canada, including wind erosion, livestock, incomes, farm management, crop  
92 production, and prices. In addition, the sparse snow cover and high spring  $T_s$  resulted in little or no spring  
93 runoff from Prairie watersheds in 1988, such that the mean runoff volume was 60% to 70% of normal  
94 (Wheaton et al., 1992). Furthermore, the 1999 – 2005 drought which was at its most severe between 2001  
95 – 2002 was felt across Canada but concentrated on the Prairies, and cost the regional economy an estimated  
96 \$3.6 billion in lost agricultural output (Council of Canadian Academies, 2013).

97 The uncertainty of drought characterization in Canada in an era of changing climate and increasing  
98 pressure from competing water users poses a major challenge to sustainable water management. A better  
99 understanding of the spatial distribution of drought, and its frequency, intensity and duration is thus  
100 required. Increased knowledge of these drought characteristics and their relationship to large-scale ocean–  
101 atmosphere forcing is necessary for predicting seasonal drought severity, as well as for planning for impacts



102 due to future climate change. Previous studies have documented significant links between low-frequency  
103 internal climate variability and Canadian hydroclimate. For example, positive phases of the Pacific Decadal  
104 Oscillation (PDO) and El Niño–Southern Oscillation (ENSO) have been associated with warm winter  $T$  in  
105 western and central Canada (Bonsal et al., 2001; Shabbar and Yu, 2012; Shabbar and Khandekar, 1996) and  
106 a reduction of snow cover in western Canada (Brown and Braaten, 1998). A review of the association of  
107 large-scale variability and low streamflows over Canada was made by Bonsal and Shabbar (2008). They  
108 found a higher frequency of low-flow events to coincide with warmer/drier conditions during El Niño  
109 events and positive phases of the PDO and the Pacific North American (PNA) pattern. Nazemi et al. (2017)  
110 investigated the major drivers of annual streamflow variability in the headwaters of the Canadian Prairies  
111 during the 20<sup>th</sup> century and found the PDO to significantly determine monotonic trends and shifts in the  
112 central tendency of annual mean streamflow.

113 Fleming and Quilty (2006) quantified the effects of organized modes of climate variability upon  
114 groundwater resources, by examining the influence of ENSO on water levels in shallow aquifers in British  
115 Columbia. They found water levels to be above average during La Niña years and below average during El  
116 Niño years, an indication of variability in winter and spring  $P$  that recharges the aquifer systems. Similarly,  
117 Tremblay et al. (2011) analyzed the variability of groundwater systems for three different regions across  
118 Canada and their linkage to the North Atlantic Oscillation (NAO), the Arctic Oscillation (AO), the PNA,  
119 and ENSO. Their findings indicated that groundwater variability in the Prince Edward Island region is  
120 mostly modulated by the NAO and AO, in Manitoba it is influenced by the PNA, while for Vancouver  
121 Island NAO, AO, and ENSO showed the highest influence. Perez-Valdivia et al. (2012) found variability  
122 in groundwater levels in the Canadian Prairies in the 2–7 and 7–10 year bands to be highly influenced by  
123 ENSO while oscillation modes in the 18–22 year band reflected a negative correlation with the PDO index.

124 The development of a comprehensive drought monitoring system capable of providing early warning  
125 of a drought's onset, severity, persistence, and spatial extent in a timely manner is a critical component in  
126 establishing a national drought policy or strategy. However, such nation-wide drought assessments in  
127 Canada are hampered partly by observational uncertainties. The paucity and heterogeneous distribution of



128  $P$  and  $T$  estimates are an important limitation for drought characterization. Ground-based measurements  
129 (e.g. gauges) are limited especially over the Rocky Mountains and north of the 60<sup>th</sup> parallel, and suffer from  
130 inaccuracies associated with cold climate processes (Wang and Lin, 2015; Wong et al., 2016; Asong et al.,  
131 2017; Asong et al., 2016a). For this purpose, it is worthwhile to study the long-term time series of  $P$  and  $T$   
132 regarding their nonhomogeneous climatic and hydrological properties. It is also important to identify  
133 homogeneous regions within Canada with distinct drought features for improved drought risk assessment  
134 and for a more efficient water resources management at the regional level. So far, most studies on droughts  
135 have been limited to Canada south of 60°N (Masud et al., 2015; Bonsal et al., 2013; Dibike et al., 2017).  
136 Nevertheless, we have not come across studies that attempt to establish the link between nation-wide  
137 drought characteristics (e.g. spatial structure, temporal patterns, periodicities) with the large-scale ocean-  
138 atmospheric modes of variability in a comprehensive manner.

139 This study aims to fill these gaps by providing a comprehensive analysis of historical droughts over  
140 the whole of Canada. Drought events are characterized by the Standardized Precipitation-  
141 Evapotranspiration Index — SPEI (Vicente-Serrano et al., 2010) over various temporal scales (1, 3, 6, and  
142 12 consecutive months, and 6 months from April to September, and 12 months from October to September).  
143 First, trends in the SPEI are investigated by means of the Mann Kendall test. Major patterns of long-term  
144 change, and periodicity of drought events are then characterized using the Rotated Empirical Orthogonal  
145 Function, and Continuous Wavelet Transform techniques, respectively. In addition, potential key drivers  
146 of drought are investigated using Wavelet Coherence analysis, with a special emphasis on the role played  
147 by large-scale modes of climate variability. Finally, due to the uncertainty associated with climate variables  
148 especially in the northern and mountainous regions where ground-based measurements are inevitably  
149 limited (Zhang et al., 2000), this study utilizes and compares two common Canada-wide gridded data sets  
150 (monthly  $P$  and  $T$ ) for the period 1950 – 2013.

151 The paper is organized as follows. Section 2 provides a description of the data and analysis methods.  
152 Section 3 discusses the detailed characteristics of drought over different regions of Canada by applying the  
153 different aforementioned statistical analyses to the drought index. This section also discusses the physical



154 and dynamical mechanisms driving the observed dry episodes in the country. Finally, a summary and  
 155 conclusions are given in Section 4.

## 156 **2 Materials and Methods**

### 157 **2.1 Study area**

158 The study area comprises the entire Canadian landmass (Fig.1). The region includes several major  
 159 river systems including the Great Lakes – St. Lawrence River system, which is one of the largest freshwater  
 160 resources globally. Topography plays an important role in shaping regional climates ranging from wet  
 161 maritime on the coasts, to dry continental across the Prairies and Boreal Plain. Snowfall is restricted to  
 162 winter months (approximately October to April depending on region). The occurrence, intensity, and timing  
 163 of seasonal  $P$  greatly influence the functioning of ecosystems in various terrestrial ecozones in this region  
 164 (Hogg et al., 2000). Based on the period 1950 – 2013, mean annual  $P$  varied from more than 2460 mm on  
 165 the west and 1260 mm on the east coasts regions, to less than 360 mm in the interior Prairie (southern  
 166 central) and northern (above 60°N) regions (Fig. 2). The long-term monthly (January – December)  
 167 minimum and maximum  $T$ s ranged from  $-30$  to  $+15^{\circ}\text{C}$  (see Section 2.2 below for data sources).  
 168 Characterized by a highly variable hydroclimate and diminishing water resources, southern parts of Canada  
 169 are home to cities with the highest population densities and support a vibrant agro-based economy that was  
 170 hard-hit by the most severe and prolonged droughts of 1988, 1999 – 2005 and 2015, as well as severe floods  
 171 of 2011, 2013 and 2014 (Wheater and Gober, 2015; Pomeroy et al., 2016).

### 172 **2.2 Data sources**

#### 173 **2.2.1 Gridded observations—ANUSPLIN**

174 The Australian National University Spline (ANUSPLIN) implementation of trivariate thin plate  
 175 smoothing splines (Hutchinson et al., 2009) has been used to provide gridded climate data over continental  
 176 Canada available on a 0.0833 grid spacing ( $\sim 10\text{-km}$ ). Variables include monthly minimum  $T$  ( $T_{\min}$ ),  
 177 maximum  $T$  ( $T_{\max}$ ) and  $P$  amounts. Station data from Environment and Climate Change Canada observing  
 178 sites were interpolated onto the high-resolution grid using the ANUSPLIN smoothing splines with  
 179 longitude, latitude, and elevation as interpolation predictors (McKenney et al., 2011). Prior to interpolation,



180 observed station data were quality controlled and corrected for station relocation, changes in the definition  
 181 of the climate day, and trace  $P$  amounts. Hopkinson et al. (2011) showed that annual mean absolute  
 182 interpolation errors in ANUSPLIN were limited to 1.0°C for  $T_{\max}$ , 1.3°C for  $T_{\min}$ , and about 9% for annual  
 183  $P$  over southern Canada.

#### 184 **2.2.2 Gridded observations—CANGRD**

185 The Canadian gridded (CANGRD) data originate from the Second Generation of Daily Adjusted  
 186 Precipitation and Temperature Data for Canada (<http://open.canada.ca/data/en/dataset/d6813de6-b20a-46cc-8990-01862ae15c5f>) with over 330 locations for  $T$  and 460 for total  $P$  (note that these numbers are  
 187 not constant over time). These data have been quality controlled and adjusted to account for known changes  
 188 in measurement practices. In particular, records from stations separated by less than 10-km were merged  
 189 so that correlations between stations would be small. See Mekis and Vincent (2011) for a detailed discussion  
 190 on merging techniques and trends in the mean climatologies of these data. For CANGRD, these data were  
 191 interpolated to evenly spaced (50-km) grids using Gandin's optimal interpolation (Gandin, 1966) technique.  
 192 As in the case of ANUSPLIN, monthly  $P$ ,  $T_{\max}$  and  $T_{\min}$  values were extracted from 1950 – 2013 and  
 193 used in the analyses.

#### 195 **2.2.3 Teleconnection indices**

196 To analyze the key drivers of drought events over Canada, six large-scale climate anomalies that have  
 197 been linked to hydroclimatic variability over Canada (Shabbar and Khandekar, 1996; Asong et al.,  
 198 2015; Zhao et al., 2013; Perez-Valdivia et al., 2012; Bonsal and Shabbar, 2008; Fleming and Quilty,  
 199 2006; Nazemi et al., 2017) and/or North America (Ropelewski and Halpert, 1986) are investigated. They  
 200 include the Pacific Decadal Oscillation (PDO) (Mantua and Hare, 2002), North Atlantic Oscillation (NAO)  
 201 (Hurrell and Van Loon, 1997), Pacific-North American (PNA) (Barnston and Livezey, 1987), Arctic  
 202 Oscillation (AO) (Zhou et al., 2001), Atlantic Multidecadal Oscillation (AMO) (Enfield et al., 2001), and  
 203 Multivariate El Niño/Southern Oscillation Index (MEI) (Wolter, 1987; Wolter and Timlin, 2011). Monthly  
 204 values of all indices are sourced from <https://www.esrl.noaa.gov/psd/> for the period 1950 – 2013.





### 205    **2.3    Drought index calculation and drought identification**

206            Many quantitative metrics have been developed and used for identification and monitoring of  
 207    droughts (Mishra and Singh, 2011; Raible et al., 2017). A variety of these indices measure, in most cases,  
 208    how much  $P$  and  $T$  for a given period deviate from historical averages. Examples include the Palmer drought  
 209    severity index (Palmer, 1965), Palmer hydrological drought index (Palmer, 1965), self-calibrated Palmer  
 210    drought severity index (Wells et al., 2004), standardized precipitation index —SPI (McKee et al., 1993),  
 211    the SPEI (Vicente-Serrano et al., 2010), and multivariate standardized drought index (Hao and  
 212    AghaKouchak, 2013). In Canada, most drought analyses (Dibike et al., 2016; Masud et al., 2017) have  
 213    utilized climate-based indices since the  $T$  and  $P$  variables are readily available for longer periods and span  
 214    larger areas, compared to hydrologic variables such as soil moisture and streamflow. In this study, we make  
 215    use of the SPEI as a meteorological proxy for drought quantification.

216            As detailed in Vicente-Serrano et al. (2010), the SPEI is a multi-scalar drought index based on a water  
 217    balance approach that uses the monthly difference between  $P$  and potential evapotranspiration (PET) to  
 218    analyze wet/dry spells over multiple time scales. SPEI involves the calculation of monthly PET, and then  
 219    subtracting this from the corresponding monthly  $P$  to obtain the climatic water balance. Several derivations  
 220    have been put forth for calculating PET, including the widely used Penman (Penman, 1948), Thornthwaite  
 221    (Thornthwaite, 1948), Priestley-Taylor (Priestley and Taylor, 1972) and Hargreaves (Hargreaves et al.,  
 222    1985) methods. However, most of these approaches require long records for solar radiation,  $T_s$ , wind speed,  
 223    and air pressure which are not readily available in Canada and many regions of the world. The Hargreaves  
 224    method (Hargreaves, 1994) which simply uses  $T_{min}$  and  $T_{max}$  for estimating PET is employed in this  
 225    study. Once PET is calculated, the difference between  $P$  and PET for the month  $j$  is calculated as in Eq.  
 226    (1):

$$Q_j = P_j - PET_j \quad (1)$$

227    where  $Q_j$  values represent monthly water surplus or deficit.



228 To compute SPEI, the monthly  $Q_j$  values are first standardized with respect to the long-term monthly  
229 mean values. One-month SPEI is generally representative of meteorological drought, while time scales  
230 between 3 and 6 months are considered as an agricultural drought index. Longer scales such as 6 and 12  
231 months are used to represent hydrological drought, and are useful for monitoring surface water resources  
232 (Beguería et al., 2014; Hayes et al., 2011). To ascertain the variability of spatiotemporal patterns for  
233 different types of droughts, the SPEI was used at different time scales, namely, at 1 (SPEI1), 3 (SPEI3), 6  
234 (SPEI6), and 12 (SPEI12) consecutive months from January – December; at 6 months during the warm  
235 season (April – September, SPEI6<sub>Apr-Sept</sub>); and at 12 months during the hydrologic year (October –  
236 September, SPEI12<sub>Oct-Sept</sub>). SPEI1, SPEI3, SPEI6, and SPEI12 account for the sub-annual variability of  
237 droughts while SPEI6<sub>Apr-Sept</sub> and SPEI12<sub>Oct-Sept</sub> account for the inter-annual variability. A drought event  
238 occurs any time the SPEI is continuously negative and reaches an intensity of -1.0 or less, and ends when  
239 SPEI becomes positive. Whenever a drought event has been detected with a start and termination month,  
240 drought properties such as duration, magnitude and frequency can be determined. SPEI categories are  
241 shown in Table 1. Unless indicated, we focus mostly on other SPEI time scales except SPEI1 which at one  
242 month is mainly a meteorological drought index.

## 243 2.4 Trend Analysis

244 Long-term trends in drought intensity and variability (inter-annual) are analyzed using the SPEI time  
245 series at each grid point. This enables investigation of the percentage of grid points with  
246 increasing/decreasing trends during the period 1950–2013 based on the ANUSPLIN- and CANGRD-  
247 derived SPEI values. Pre-whitening as described in Yue et al. (2002) is first applied to the monthly SPEI  
248 anomalies to remove lag-1 auto-correlation, since serial correlation is generally recognized to influence  
249 trends in auto-correlated time series, which may distort the power of Mann-Kendal test. Pre-whitening is  
250 limited to a low order autoregressive model, i.e., AR(1), since it can falsify the structure of variability in  
251 time series across time scales (particularly with higher order models) (Razavi and Vogel, 2018). The pre-



whitened SPEI values on different time scales are then used for detecting statistically significant ( $p < 0.05$ ) trends on a pixel basis. Further details on Mann–Kendall trends can also be found in Hamed and Rao (1998).

## 2.5 Empirical Orthogonal Function Analysis

Hydro-climatological data are often characterized by non-linearity and high dimensionality. Thus, the challenging task is to find ways to reduce the dimensionality of the system to as few modes as possible by expressing the data in such a way as to highlight their similarities and differences (Hannachi et al., 2007). Empirical Orthogonal Function (EOF) analysis (also known as principal component analysis—PCA) is among the most widely and extensively used method in hydroclimate sciences for accomplishing such tasks (Richman, 1986; Wilks, 2011; Preisendorfer and Mobley, 1988). EOF is employed to find hydroclimate sub-regions that experienced similar drought features during the period 1950–2013. The EOF consists of computing the covariance matrix of the SPEI series with the corresponding eigenvalues and eigenvectors (Uvo, 2003).

Following the rule by North et al. (1982), the sampling errors at 95% confidence level of the eigenvalues associated with the leading components were estimated in order to establish how many modes to retain for rotation. To achieve more stable and physically explainable patterns, a rotation of the retained components with the varimax procedure (Richman, 1986) was applied. The patterns defined in this way are referred to as rotated empirical orthogonal functions (REOF). In summary, the REOF (spatial patterns) values indicate the spatial representativeness of each rotated temporal component—RPC (temporal patterns). Subsequently, we obtained the most revealing patterns of drought evolution across Canada and determined the spatial extent of each component series by mapping the factorial matrix values (i.e. correlation between each REOF and the original SPEI series). Finally, the time variability of the selected RPCs of SPEI were examined for possible trends in the identified sub-regions using linear regression. The slopes of the trends were computed by applying the method of least squares linear fitting to the time series.

## 2.6 Wavelet Analysis

After delimitating hydroclimate sub-regions that experienced similar drought features, the RPC time series corresponding to the REOFs was then analyzed in a time-frequency domain (to reveal dominant



oscillations) by means of the continuous wavelet transform (CWT). Subsequently, by utilizing the wavelet coherence (WCO) technique (Grinsted et al., 2004; Torrence and Compo, 1998; Addison, 2016), the relationships between the dominant oscillations and large-scale climate indices that have possibly modulated historical drought patterns across Canada are investigated. The CWT projects the spectral-temporal characteristics of a time series onto a time-frequency plane from which the dominant periodicities and their duration can be distinguished (Fugal, 2009; Grinsted et al., 2004).

The wavelet power spectrum (WPS) is defined as the squared modulus of the CWT (Jiang et al., 2014; Hao et al., 2012), and represents the signal energy at a specific scale (period) and time. From the WPS, the various periodicities and the time intervals of their occurrence can be determined. For a given time series  $\{y_n\}$ , with  $n = 1, 2, 3, \dots, N$ , the CWT is given by:

$$W_n(s) = \sum_{n'=1}^N \left( \frac{\delta t}{s} \right)^{0.5} y_{n'} \psi^* \left[ \frac{(n' - n) \delta t}{s} \right] \quad (2)$$

where  $W_n(s)$  are the wavelet coefficients,  $n$  is the time index describing the location of the wavelet in time,  $s$  is the wavelet scale, and  $\delta t$  is the sampling interval. The function  $\psi$  is the mother wavelet, and the asterisk (\*) denotes its complex conjugate. The Morlet wavelet was used since it provides a good balance between time and frequency domains and is suitable when the purpose is to extract dominant signals (Grinsted et al., 2004). The statistical significance of the CWT was assessed against a red noise background at a 95% confidence interval. The CWT function creates a cone of influence (COI) that delimitates a region of the WPS beyond which edge effects become important and the power could be suppressed (Torrence and Compo, 1998).

Wavelet analysis can also be used to identify the covariance between two time series. This can be done using the concept of wavelet coherence (Grinsted et al., 2004). Wavelet coherence (WCO) reveals local similarities between two time series and may be considered a local correlation coefficient in the time-frequency (time-period) plane. For climatological time series, WCO can be used to identify their possible



teleconnection with large-scale atmospheric drivers. The WCO between two time series can be computed by normalizing and smoothing their cross wavelet spectrum:

$$W_n^{XY}(s) = W_n^X(s)W_n^{Y*}(s) \quad (3)$$

where  $W_n^X(s)$  and  $W_n^Y(s)$  represent the WPS of the time series  $\{x_i\}$  and  $\{y_i\}$ , respectively. The statistical significance ( $p < 0.05$ ) of the WCO is estimated using Monte Carlo methods with respect to a red-noise spectrum resulting in significant periodicities of coherence delineated by significance contours. As in the CWT, regions outside of the COI should be interpreted with caution (Torrence and Compo, 1998).

### 3 Results and discussion

#### 3.1 Spatial structure of long-term climatic water balance

Fig. 3 shows the average monthly (January – December) water surplus/deficit (mm) as defined in Eq. (1) for ANUSPLIN and CANGRD. It is evident that, apart from the Pacific/Atlantic maritime, most of the continental Canadian interior experienced moisture deficits, with the Prairie being the most affected region (this region also has the highest climatological  $T_{min}$  and  $T_{max}$ , and some of the least mean annual  $P$  during the study period—Fig. 2). Other than the coastal areas, there is a general east to west moisture deficit pattern, mostly determined by the  $P$  and  $T$  pattern. For comparison, 5.8% (33.3%) of CANGRD points experienced moisture surplus (deficit), and 4.3% (41.6%) for ANUSPLIN. This implies that ANUSPLIN showed a relatively higher tendency towards dryness relative to CANGRD.

#### 3.2 Long-term trends

Fig. 4 depicts the spatial structure of long-term (1950 – 2013) SPEI trends at various time scales. Only grid points with significant trends are shown. It is noteworthy that significant trends largely occur in spatially isolated blocks. Decreasing trends are observable in the southern parts of the Prairies, the foothills of the Rocky Mountains and Pacific maritime regions, whereas increasing trends are limited to a small area in the north, and parts of Atlantic coast to the east, similar to the water balance shown in Fig. 3.

Table 2 shows the percentage of grids with decreasing and increasing trends for ANUSPLIN and CANGRD. For both data sets, the percentage generally decreases with increasing SPEI time scale.



ANUSPLIN has a higher tendency towards dryness (decreasing trends) unlike CANGRD. Using SPEI12 as an example, 10% of ANUSPLIN pixels experienced decreasing trends compared to 4% in the case of CANGRD. Conversely, apart from SPEI1, CANGRD showed a strong tendency towards wetness (increasing trends) relative to ANUSPLIN. These differences can be attributed partly to the inputs (e.g. the number of stations considered for gridding ANUSPLIN is larger than the number of stations of the CANGRD dataset), estimation methods and spatial resolution which are different for both data sets (see Section 2.2).

### 3.3 Spatial patterns of drought

Concerning the EOF analysis, and taking into account the percentage of variance explained by each rotated component (REOF), two main patterns were identified for subsequent discussion and analysis. Table 3 presents the explained variances of varimax rotated components relative to the considered SPEI time scales and data sets. The first two components (for both data sets) explain about 28% to 33.9% of the total variance depending on the time scale, with the minimum and maximum variances observed for SPEI1 and SPEI12, respectively, in the case of ANUSPLIN. For CANGRD, SPEI6<sub>Apr-Sept</sub> and SPEI12 explained the minimum and maximum variances, respectively.

Fig. 5 shows that between the two main components (REOF), the regions with higher correlations (>0.7) do not overlap, with clearly spatially disjunctive structure. For all SPEI time scales, the loading patterns of the first component (REOF1) with a maximum explained temporal variance of 20.6% (SPEI12, ANUSPLIN) and 19.5% (SPEI1, CANGRD) highlights mainly the drought evolution on the interior Prairie ecozone of Canada. This semi-arid region is relatively low-lying and characterized by high hydroclimate variability and some of the least annual mean *P*. The second component (REOF2) explains a maximum variance of around 13.8% (SPEI3) in the case of ANUSPLIN and 13.1% (SPEI12<sub>Oct-Sept</sub>) for CANGRD. REOF2 is mainly representative of the Northern central part of Canada (with the least annual mean *P*), including the Taiga Shield, Taiga Plains, Southern Arctic, and Taiga Cordillera ecozones, with positive correlations across all time scales and data sets. In summary, the foregoing analyses suggest that the Prairies and Northern central regions are the leading droughts modes for Canada, in that they are well captured by the two data sets with high positive loadings at all investigated time scales.



### 3.4 Temporal drought characteristics

The RPCs of REOF1 and REOF2 for ANUSPLIN and CANGRD, as well as correlation coefficients between the data sets, are shown in Fig. 6. It is evident that the RPCs from the two data sets are strongly correlated ( $cor > 0.75$ ) for all SPEI time scales, except for RPC2 of SPEI3 where  $cor = 0.45$  (the centroids of SPEI3 REOF2 in Fig. 5 are slightly different for both data sets). Primary focus is on SPEI6<sub>Apr-Sept</sub> and SPEI12<sub>Oct-Sept</sub> which reflect the agricultural season (when droughts are most critical for rain-fed and irrigated agriculture), and hydrological year in Canada, respectively. Fig. 6 reveals that the Prairies (REOF1 and RPC1) experienced moderate to extreme (Table 1) drought episodes starting in the mid 1950s, early and late 1960s, the 1970s and 1980s, the period from mid 1997 – 2005, and the summer of 2009. Some of the drought episodes were extremely dry and severe as they were prolonged in time such as the one in the late 1970s, mid 1980s, and 1997 – 2005. These identified drought events correspond well with the findings of Bonsal et al. (2011) who identified large-scale Prairie droughts in 1961, 1967, 1988, and 2001 using ANUSPLIN and CANGRD data. In the Northern central region (REOF2 and RPC2), although fewer droughts were detected for the hydrological year (SPEI12<sub>Oct-Sept</sub>) with the most intense occurring in 2000 (based on the ANUSPLIN data set), the seasonal SPEI series (SPEI6<sub>Apr-Sept</sub>) detected several drought events in this region. Extremely dry episodes in this region occurred in the early 1960s, 1980s, early 1990s and 2000s.

Linear trends of the RPCs for the two sub-regions are depicted in Fig. 7 and Table 4. For the Prairie sub-region, both ANUSPLIN and CANGRD showed insignificant decreasing trends for SPEI6, SPEI6<sub>Apr-Sept</sub> and SPEI12<sub>Oct-Sept</sub>. However, in the Northern central region, the trend direction is not the same for both data sets at all SPEI time scales. For ANUSPLIN (CANGRD), decreasing (increasing) trends are found in SPEI6<sub>Apr-Sept</sub>. Conversely, CANGRD (ANUSPLIN) shows decreasing (increasing) trends in SPEI3. Regionally, SPEI at different time scales tend to display more significant trends in the Northern central relative to the Prairies. Most of the trends are significant in the case of CANGRD compared to ANUSPLIN. The apparent differences in trends between the two data sets and sub-regions may be attributed to the low



station density in areas above 60°N which can introduce higher uncertainty in the gridded  $P$  and  $T$  fields  
 (Vincent et al., 2015).

### 3.5 Frequency estimation/periodicity of drought

To detect the dominant frequencies in the RPCs of the SPEI series in Fig. 6, the time series were  
 further analyzed using a CWT. The wavelet power spectrum (WPS) of the RPCs is shown in Fig. 8.  
 Periodicities of drought will be identified for SPEI6<sub>Apr-Sept</sub> and SPEI12<sub>Oct-Sept</sub> and their relationship to  
 teleconnection indices examined. These two time scales correspond to the warm season and water year,  
 respectively, and represent periods when moisture shortages are most critical for various sectors in Canada.  
 Other SPEI time scales which explain sub-annual variability are included in Fig. 8 for the interested reader.  
 For SPEI6<sub>Apr-Sept</sub>, from the WPS of RPC1 in Fig. 8, significant interannual variability of between 8 and 32  
 months is evident throughout much of the entire lengths of the SPEI time series, coinciding with 2–6 year  
 frequencies usually associated to ENSO, e.g., (Shabbar and Skinner, 2004; Gobena and Gan, 2006).  
 However, it is concentrated most heavily during the mid 1950s, early and late 1960s, the 1970s and 1980s,  
 the period from mid 1997 – 2010. For SPEI12<sub>Oct-Sept</sub>, a strong frequency band is centered mostly around 16  
 – 66 months (~4 years), and concentrated during the mid 1950s and late 1960s. Moreover, 32 – 64 months  
 frequencies are dominant in the mid 1980s, and the years between 1990 – 2010.

In the Northern central region (RPC2), for SPEI6<sub>Apr-Sept</sub>, significant periodicity of between 8 – 40  
 months cycle as a dominant period of variability is evident. It is concentrated in the early 1960s, 1980s, late  
 1990s, and 2000s. For SPEI12<sub>Oct-Sept</sub>, the WPS indicates a significant high power for relatively low-  
 frequency (16 – 100 months, i.e. ~7 years) signals, concentrated over the period 1956 – 1975 and 1995 –  
 2013. The foregoing analysis reveals that the Prairie region (REOF1) of Canada is dominated by high-  
 frequency power signals with high cycles of oscillation for both SPEI6<sub>Apr-Sept</sub> and SPEI12<sub>Oct-Sept</sub>, while the  
 northern central region (REOF2) is dominated by relatively low-frequency power signals and low cycles  
 of oscillation. The analysis further indicates that significant interannual periodicities (<10 years) dominate  
 drought variability over the two identified sub-regions across Canada. The dominant periodicities and the  
 intervals during which they occurred are summarized in Table 5.





### 3.6 Coherence between drought and large-scale climate drivers

The WCO technique was used to identify both frequency bands and time intervals at which  $\text{SPEI6}_{\text{Apr-Sep}}$  and  $\text{SPEI12}_{\text{Oct-Sep}}$  and large-scale climate indices are covarying (Torrence and Webster, 1999). The results of WCO coefficients between the RPCs of  $\text{SPEI6}_{\text{Apr-Sep}}$  and  $\text{SPEI12}_{\text{Oct-Sep}}$  and teleconnection indices are shown in Figs. 9 – 11. In these plots, the coloured shading represents the magnitude in the coherence as shown in the colour bar, which varies from 0 to 1 and indicates the time scale variability in the correlation between the two time series. As in Fig. 8, the black contours represent the significant regions. The relative phase relationships are shown as arrows, with in-phase pointing right (positive correlation), and anti-phase pointing left (negative correlation), whereas a vertically up (down) arrow indicates that the second time series lags (leads) the first in phase by  $90^\circ$ . If association exists between two time series, a slowly varying phase lag would be expected, and the phenomena would be phase locked, i.e., phase arrows point only in one direction for a given wavelength (Grinsted et al., 2004; Gobena and Gan, 2006). For this study, phase angle associations were noted strictly as either being in-phase or antiphase locked. To simplify and limit the length of the paper, only results for large-scale climate indices having the strongest correlations with frequencies of drought are shown. Other results are included as supplementary material.

Fig. 9 illustrates the squared WCO between the temporal patterns of drought and MEI. It is apparent that, for  $\text{SPEI6}_{\text{Apr-Sep}}$ , the MEI had significant coherence with PC1 mainly concentrated in the 8 – 16 months band and from 1960 – 1980 in the Prairie region, indicating that the two time series are phase-locked over this time interval. Also, the strongest coherence between PC1 and MEI occurred over the 32–50 month scale, spanning the period 1986 – 2002. In the case of  $\text{SPEI6}_{\text{Apr-Sep}}$  PC2 (Northern central region), discontinuous in-phase coherence patterns were detected in the 2 – 32 months bands. The dominant high energy coherence occurred in the 16 – 32 month scale, spanning the period 1985 – 2005. Similarly, for the hydrological year time scale ( $\text{SPEI12}_{\text{Oct-Sep}}$ ), drought in the Prairies ( $\text{SPEI12}_{\text{Oct-Sep}}$ PC1) experienced significant high power with the MEI at the 16 – 32 month scale from 1980 – 2005 based on ANUSPLIN (1986 – 2005 based on CANGRD). Whereas, in the Northern central region ( $\text{SPEI12}_{\text{Oct-Sep}}$ PC2), significant in-phase cross power between drought and the MEI occurred at the 32 – 64 month period over the years



1978 – 2000 (in the case of ANUSPLIN). As in Fig. 8, it can be seen that the Prairie region has more short-term periodicities, compared to the Northern central region. It is also evident that although the MEI co-varied with drought events, the frequency is higher but short-lived in the Prairies relative to the Northern central region.

Fig. 10 shows that for both the seasonal ( $\text{SPEI6}_{\text{Apr-Sep}}$ ) and annual ( $\text{SPEI12}_{\text{Oct-Sep}}$ ) drought time series, sporadic but significant coherence is observed intermittently from year-to-year with the PDO. For  $\text{SPEI6}_{\text{Apr-Sep}}$ , dominant strong coherence occurred between 16 – 32 months over the period 1988 – 2003 for the Prairies region, whereas fluctuation was intermittently observed between 1955 – 2000 for  $\text{SPEI12}_{\text{Oct-Sep}}$  over the Prairie and Northern central regions ranging from 16 – 64 months. Unlike the PDO, the PNA showed strong in-phase relationship with drought over Canada (Fig. 11). It is apparent that the PNA co-varied significantly with  $\text{SPEI6}_{\text{Apr-Sep}}\text{PC1}$  over most of the years during the study period. Oscillations in the PNA are manifested in the  $\text{SPEI6}_{\text{Apr-Sep}}\text{PC1}$  on wavelengths varying from 2–108 months (~9 years), suggesting that the PNA actively mirrors  $\text{SPEI6}_{\text{Apr-Sep}}\text{PC1}$ . Particularly, the PNA was phase-locked with drought during the period 1980 – 2001 at 16 – 32 months scale. Apart from the late 1990s and early 2000s at the 8 – 16 months scale, no significant coherence was found between the PNA and  $\text{SPEI6}_{\text{Apr-Sep}}\text{PC2}$ . Although with less coherence relative to  $\text{SPEI6}_{\text{Apr-Sep}}$ , the PNA also co-varied with  $\text{SPEI12}_{\text{Oct-Sep}}$ , more so for the Northern Central region compared to the Prairie region. In the Prairie region, the strongest coherence between  $\text{SPEI12}_{\text{Oct-Sep}}\text{PC1}$  and the PNA occurred over the 16–32 months scale, while for the Northern central region, significantly cross power between the PNA and  $\text{SPEI12}_{\text{Oct-Sep}}\text{PC2}$  occurred over the 32 – 64 months scale, spanning the periods 1960 – 1973 and 1985 – 2000.

The relationship between drought and the AMO is shown in Fig. S1. It is clear that the AMO did not co-vary with  $\text{SPEI6}_{\text{Apr-Sep}}$  over both homogenous drought regions. However, it is important to note that Shabbar and Skinner (2004) found significant correlation pattern between the winter AMO index and following summer PDSI in the north of the Prairies provinces. Here, we only made use of the AMO index for the months April – September of each year. For  $\text{SPEI12}_{\text{Oct-Sep}}$ , significant and high-energy existed for the Prairie region only ( $\text{SPEI12}_{\text{Oct-Sep}}\text{PC1}$ ) and mainly distributed in the 8 – 64 months (~5 years) band and



spanning the period 1970 – 2005. For the AO (Fig. S2), in-phase significant coherence existed with SPEI6<sub>Apr-Sept</sub> PC2 and SPEI12<sub>Oct-Sept</sub> PC1. In the Northern central region (SPEI6<sub>Apr-Sept</sub> PC2), 16 – 32 months high-energy regions in this band were found over the period 1963 – 1978, and 8 – 16 months significant coherence also existed from 1994 – 2002. In the Prairie region (SPEI12<sub>Oct-Sept</sub> PC1), drought was in-phase with the AO especially from 1981 – 2003 where significant cross power and coherence mainly concentrated in the 64 – 128 months band (based on CANGRD). The results further indicate that the AO was in anti-phase with SPEI6<sub>Apr-Sept</sub> PC1 and SPEI12<sub>Oct-Sept</sub> PC2 during the study period from 1950 – 2013. In terms of the NAO (Fig. S3), sporadic significant coherence is noticed with the seasonal SPEI6<sub>Apr-Sept</sub> at higher frequency ranging between 4 – 20 months and mainly concentrated over the period 1975 – 1990. There are also statistically significant in-phase coherence between SPEI12<sub>Oct-Sept</sub> PC1 and the NAO at around 70 – 128 months band in the late 1970s – late 1990s, based on CANGRD.

The foregoing analysis have shown significant covariance between drought variability over Canada and large scale climate indices, especially the MEI, PNA and PDO. This is in line with previous studies e.g. (Bonsal and Shabbar, 2008; Fleming and Quilty, 2006; Tremblay et al., 2011; Perez-Valdivia et al., 2012) that have established links between Canadian hydroclimate and teleconnection indices. Furthermore, one should expect most of the climate indices to yield similar findings given that they appear to be interrelated at several time scales (Sheridan, 2003; Gan et al., 2007; Ng and Chan, 2012). We recommend that future studies examine the degree to which such interrelations can affect the findings reported here by eliminating, for example, the influence of the PDO on the MEI via partial wavelet coherence analysis (Ng and Chan, 2012). Also, a lead/lag response of the identified drought frequencies as well their correlations to positive and negative phases of various teleconnections constitute an area for future research.

#### 4 Summary and conclusions

This study performs a comprehensive analysis of historical droughts over the whole of Canada, considering the role teleconnections by analyzing different monthly *P* and *T* products for the period 1950 – 2013. SPEI, a climatological drought index, is applied over various temporal scales to evaluate various drought characteristics such as trends, spatiotemporal patterns of long-term change, inter/intra-annual



variability, and periodicity/frequency. In addition, potential prominent modes of low-frequency variability such as the PNA, AO, MEI, PDO, AMO and NAO which are well established to influence the hydroclimate of Canada and North America are investigated as precursors to historical drought occurrence. The main conclusions from the analyses are:

- Apart from the Pacific/Atlantic maritime regions, most of the continental Canadian interior experienced moisture deficits, with the Prairie region being the most affected region between 1950 – 2013. Based on a trend analysis derived from the water balance, significant decreasing trends in SPEI values are observed in the southern Prairies, the foothills of the Rocky Mountains and Pacific maritime regions, whereas increasing trends are limited to a small area in the north, and parts of Atlantic coast to the east. Therefore, southern parts of the country showed a trend towards drier conditions and vice versa for the northern regions. Note that the northern region (above 60°N) has lower station density and as such higher uncertainty in the gridded  $P$  and  $T$  fields.
- EOF identifies two main spatially disjunctive sub-regions of drought variability over Canada —the Prairie and Northern central regions. Based on both seasonal ( $\text{SPEI6}_{\text{Apr-Sep}}$ ) and annual ( $\text{SPEI12}_{\text{Oct-Sep}}$ ) SPEI values, the Prairie sub-region experienced moderate to extreme droughts episodes starting in the mid 1950s, early and late 1960s, the 1970s and 1980s, the period from mid 1997 – 2005, and the summer of 2009. Some of the drought episodes were extremely dry and severe as they were prolonged in time such as the ones in the late 1970s, mid 1980s, and 1997 – 2005. In the Northern central region, although fewer (likely due to below 0 temperatures for most of the cold season) droughts were detected for the hydrological year ( $\text{SPEI12}_{\text{Oct-Sep}}$ ) with the most intense occurring in 2000, the seasonal SPEI series ( $\text{SPEI6}_{\text{Apr-Sep}}$ ) detected extremely dry episodes in this region in the early 1960s, 1980s, early 1990s and 2000s. However, drought variability in the Prairies in particular experienced largely insignificant trends, a finding similar to numerous previous studies.
- Wavelet analysis was particularly useful to detect periodical signals in the SPEI time series patterns for each sub-region. For  $\text{SPEI6}_{\text{Apr-Sep}}$ , the analysis reveals clearly the presence of a dominant periodicity of between 8 and 32 months, persisting approximately from 1955 to 2001 in the Prairie



505 region, while in the North central region, significant periodicity of between 8 – 40 months cycle as a  
506 dominant period of variability spanning the years 1955 – 2000 is apparent. For SPEI12<sub>Oct-Sept</sub>, a strong  
507 power frequency band over the Prairie region, centered mostly around 16 – 66 months (~4 years) and  
508 spanning the period 1955 – 1968 is found. Moreover, 32 – 64 months periodic high-power signals  
509 are dominant during the years 1970 – 2002. In the Northern central region, a significant high power  
510 for relatively low-frequency (16 – 100 months, i.e. ~7 years), spanning the period 1956 – 1975 and  
511 1995 – 2013 is detected. Therefore, the Prairie region of Canada is dominated by high-frequency (i.e.  
512 more frequent and shorter cycles of dry events) power signals for both SPEI6<sub>Apr-Sept</sub> and SPEI12<sub>Oct-</sub>  
513 <sub>Sept</sub>, while the Northern central region is dominated by low-frequency (i.e. less frequent cycles of dry  
514 events) power signals. The analysis further indicates that significant interannual periodicities (with a  
515 period of <10 years) dominate drought variability over the two identified major regions of drought  
516 variability across Canada.

- 517 • The identified drought short-time (long-time) interannual periodicities in the Prairie (Northern central  
518 region) are likely associated with the immediate and significant influence of the MEI and PNA in  
519 particular as these large scale climate indices have maximum regions with a 5% significance level in  
520 the WCO plots. For the MEI index, 8 – 16 and 32 – 50 months was the most predominant and effective  
521 period on the drought occurrence in Canada, while for the PNA, 2–108 months period was the most  
522 predominant over the Prairie region and for SPEI6<sub>Apr-Sept</sub> compared with the Northern central region,  
523 while for SPEI12<sub>Oct-Sept</sub>, the PNA showed more coherence with drought in the 32 – 64 months scale.

524 The foregoing analysis has indicated the need to consider various observational data sets in drought  
525 characterization, given the uncertainty in data. In terms of trends, the ANUSPLIN data set indicated a higher  
526 tendency for drought over the study period relative to CANGRD. Furthermore, irrespective of the time  
527 scale of accumulation, ANUSPLIN tends to reveal more drought severity compared to CANGRD although  
528 the correlation between the time series of the two data sets from each of the homogenous drought sub-  
529 regions is very strong. Therefore, further applications using other gridded data sets to verify the role played  
530 by the spatial resolution of the input data on regional drought patterns are recommended. The identification



531 of these sub-regions with similar drought variability and characteristics can be useful for drought risk  
532 management at a regional scale in Canada. Two of the most important river basins are both in the Prairies  
533 region (Saskatchewan River Basin) and Northern region (MacKenzie River Basin). Lastly, this study is the  
534 first of its kind to identify dominant periodicities in drought variability over the whole of Canada in terms  
535 of when the drought events occur, the duration, and how often they do so over the Prairies and Northern  
536 central regions.

537

538

539

540

541

542

543

544

545

546

547

548

549

550

551

552

553

554

555 **5 References**

- 556 Addison, P. S.: The Illustrated Wavelet Transform Handbook: Introductory Theory and Applications in  
557 Science, Engineering, Medicine and Finance, Second Edition, CRC Press, Taylor & Francis Group, 2016.
- 558 Asong, Z. E., Khaliq, M. N., and Wheeler, H. S.: Regionalization of precipitation characteristics in the  
559 Canadian Prairie Provinces using large-scale atmospheric covariates and geophysical attributes, *Stochastic*  
560 *Environmental Research and Risk Assessment*, 29, 875-892, 10.1007/s00477-014-0918-z, 2015.
- 561 Asong, Z. E., Khaliq, M. N., and Wheeler, H. S.: Multisite multivariate modeling of daily precipitation and  
562 temperature in the Canadian Prairie Provinces using generalized linear models, *Climate Dynamics*, 47,  
563 2901-2921, 10.1007/s00382-016-3004-z, 2016a.
- 564 Asong, Z. E., Razavi, S., Wheeler, H. S., and Wong, J. S.: Evaluation of Integrated Multi-satellite  
565 Retrievals for GPM (IMERG) over Southern Canada against Ground Precipitation Observations: A  
566 Preliminary Assessment, *Journal of Hydrometeorology*, 0, null, 10.1175/jhm-d-16-0187.1, 2017.
- 567 Barnston, A. G., and Livezey, R. E.: Classification, Seasonality and Persistence of Low-Frequency  
568 Atmospheric Circulation Patterns, *Monthly Weather Review*, 115, 1083-1126, 10.1175/1520-  
569 0493(1987)115<1083:csapol>2.0.co;2, 1987.
- 570 Beguería, S., Vicente-Serrano, S. M., Reig, F., and Latorre, B.: Standardized precipitation  
571 evapotranspiration index (SPEI) revisited: parameter fitting, evapotranspiration models, tools, datasets and  
572 drought monitoring, *International Journal of Climatology*, 34, 3001-3023, 10.1002/joc.3887, 2014.
- 573 Bonsal, Shabbar, A., and Higuuchi, K.: Impacts of low frequency variability modes on Canadian winter  
574 temperature, *International Journal of Climatology*, 21, 95-108, 10.1002/joc.590, 2001.
- 575 Bonsal, and Regier, M.: Historical comparison of the 2001/2002 drought in the Canadian Prairies, *Climate*  
576 *Research*, 33, 229-242, 2007.
- 577 Bonsal, Wheaton, E., Meinert, A., and Siemens, E.: Characterizing the Surface Features of the 1999–2005  
578 Canadian Prairie Drought in Relation to Previous Severe Twentieth Century Events, *Atmosphere-Ocean*,  
579 49, 320-338, 10.1080/07055900.2011.594024, 2011b.
- 580 Bonsal, Aider, R., Gachon, P., and Lapp, S.: An assessment of Canadian prairie drought: past, present, and  
581 future, *Climate Dynamics*, 41, 501-516, 10.1007/s00382-012-1422-0, 2013.
- 582 Bonsal, B., Zhang, X., and Hogg, W.: Canadian Prairie growing season precipitation variability and  
583 associated atmospheric circulation, *Climate Research*, 11, 191-208, 1999.
- 584 Bonsal, B., and Shabbar, A.: Impacts of large-scale circulation variability on low streamflows over Canada:  
585 a review, *Canadian Water Resources Journal*, 33, 137-154, 2008.
- 586 Bonsal, B. R., Wheaton, E. E., Meinert, A., and Siemens, E.: Characterizing the Surface Features of the  
587 1999–2005 Canadian Prairie Drought in Relation to Previous Severe Twentieth Century Events,  
588 *Atmosphere-Ocean*, 49, 320-338, 10.1080/07055900.2011.594024, 2011.
- 589 Brown, R. D., and Braaten, R. O.: Spatial and temporal variability of Canadian monthly snow depths, 1946–  
590 1995, *Atmosphere-Ocean*, 36, 37-54, 10.1080/07055900.1998.9649605, 1998.
- 591 Bryant, E. A.: *Natural Hazards*, University of Cambridge UK Cambridge  
592 2005.
- 593 Council of Canadian Academies: *Water and Agriculture in Canada: Towards Sustainable Management of*  
594 *Water Resources*. Chapter 6 – Building the Foundation for Sustainable Management of Water in  
595 *Agriculture*. Available at: <http://www.scienceadvice.ca/en/assessments/completed/water-agri.aspx>, 2013.
- 596 Dai, A.: Drought under global warming: a review, *Wiley Interdisciplinary Reviews: Climate Change*, 2,  
597 45-65, 10.1002/wcc.81, 2011.
- 598 Dibike, Y., Prowse, T., Bonsal, B., and O'Neil, H.: Implications of future climate on water availability in  
599 the western Canadian river basins, *International Journal of Climatology*, n/a-n/a, 10.1002/joc.4912, 2016.
- 600 Dibike, Y., Prowse, T., Bonsal, B., and O'Neil, H.: Implications of future climate on water availability in  
601 the western Canadian river basins, *International Journal of Climatology*, 37, 3247-3263, 10.1002/joc.4912,  
602 2017.





- 603 Dracup, J. A., Lee, K. S., and Paulson, E. G.: On the definition of droughts, *Water Resources Research*, 16,
- 604 297-302, 10.1029/WR016i002p00297, 1980.
- 605 Enfield, D. B., Mestas-Núñez, A. M., and Trimble, P. J.: The Atlantic Multidecadal Oscillation and its
- 606 relation to rainfall and river flows in the continental U.S, *Geophysical Research Letters*, 28, 2077-2080,
- 607 10.1029/2000GL012745, 2001.
- 608 Fleming, S. W., and Quilty, E. J.: Aquifer Responses to El Niño–Southern Oscillation, *Southwest British*
- 609 *Columbia, Ground Water*, 44, 595-599, 10.1111/j.1745-6584.2006.00187.x, 2006.
- 610 Fugal, D. L.: *Conceptual Wavelets in Digital Signal Processing: An In-depth, Practical Approach for the*
- 611 *Non-mathematician*, Space & Signals Technical Pub., 2009.
- 612 Gan, T. Y., Gobena, A. K., and Wang, Q.: Precipitation of southwestern Canada: Wavelet, scaling,
- 613 multifractal analysis, and teleconnection to climate anomalies, *Journal of Geophysical Research:*
- 614 *Atmospheres*, 112, 2007.
- 615 Gandin, L. S.: *Objective analysis of meteorological fields*. By L. S. Gandin. Translated from the Russian.
- 616 Jerusalem (Israel Program for Scientific Translations), 1965. Pp. vi, 242: 53 Figures; 28 Tables. £4 1s. 0d,
- 617 *Quarterly Journal of the Royal Meteorological Society*, 92, 447-447, 10.1002/qj.49709239320, 1966.
- 618 Gobena, A. K., and Gan, T. Y.: Low-frequency variability in Southwestern Canadian stream flow: links
- 619 with large-scale climate anomalies, *International Journal of Climatology*, 26, 1843-1869, 10.1002/joc.1336,
- 620 2006.
- 621 Grinsted, A., Moore, J. C., and Jevrejeva, S.: Application of the cross wavelet transform and wavelet
- 622 coherence to geophysical time series, *Nonlin. Processes Geophys.*, 11, 561-566, 10.5194/npg-11-561-2004,
- 623 2004.
- 624 Hamed, K. H., and Rao, R. A.: A modified Mann-Kendall trend test for autocorrelated data, *Journal of*
- 625 *Hydrology*, 204, 182-196, [https://doi.org/10.1016/S0022-1694\(97\)00125-X](https://doi.org/10.1016/S0022-1694(97)00125-X), 1998.
- 626 Hannachi, A., Jolliffe, I. T., and Stephenson, D. B.: Empirical orthogonal functions and related techniques
- 627 in atmospheric science: A review, *International Journal of Climatology*, 27, 1119-1152, 10.1002/joc.1499,
- 628 2007.
- 629 Hao, Y., Liu, G., Li, H., Li, Z., Zhao, J., and J. Yeh, T.-C.: Investigation of karstic hydrological processes
- 630 of Niangziguan Springs (North China) using wavelet analysis, *Hydrological Processes*, 26, 3062-3069,
- 631 10.1002/hyp.8265, 2012.
- 632 Hao, Z., and AghaKouchak, A.: Multivariate Standardized Drought Index: A parametric multi-index model,
- 633 *Advances in Water Resources*, 57, 12-18, <http://dx.doi.org/10.1016/j.advwatres.2013.03.009>, 2013.
- 634 Hargreaves, G H: Defining and Using Reference Evapotranspiration, *Journal of Irrigation and Drainage*
- 635 *Engineering*, 120, 1132-1139, doi:10.1061/(ASCE)0733-9437(1994)120:6(1132), 1994.
- 636 Hargreaves, G. L., Hargreaves, G. H., and Riley, J. P.: Agricultural Benefits for Senegal River Basin,
- 637 *Journal of Irrigation and Drainage Engineering*, 111, 113-124, doi:10.1061/(ASCE)0733-
- 638 9437(1985)111:2(113), 1985.
- 639 Hayes, M., Svoboda, M., Wall, N., and Widhalm, M.: The Lincoln Declaration on Drought Indices:
- 640 Universal Meteorological Drought Index Recommended, *Bulletin of the American Meteorological Society*,
- 641 92, 485-488, 10.1175/2010bams3103.1, 2011.
- 642 Hogg, E. H., Price, D. T., and Black, T. A.: Postulated Feedbacks of Deciduous Forest Phenology on
- 643 Seasonal Climate Patterns in the Western Canadian Interior, *Journal of Climate*, 13, 4229-4243,
- 644 10.1175/1520-0442(2000)013<4229:pfodfp>2.0.co;2, 2000.
- 645 Hopkinson, R. F., McKenney, D. W., Milewska, E. J., Hutchinson, M. F., Papadopol, P., and Vincent, L.
- 646 A.: Impact of Aligning Climatological Day on Gridding Daily Maximum–Minimum Temperature and
- 647 Precipitation over Canada, *Journal of Applied Meteorology and Climatology*, 50, 1654-1665,
- 648 10.1175/2011jamc2684.1, 2011.
- 649 Hurrell, J. W., and Van Loon, H.: DECADAL VARIATIONS IN CLIMATE ASSOCIATED WITH THE
- 650 NORTH ATLANTIC OSCILLATION, *Climatic Change*, 36, 301-326, 10.1023/a:1005314315270, 1997.
- 651 Hutchinson, M. F., McKenney, D. W., Lawrence, K., Pedlar, J. H., Hopkinson, R. F., Milewska, E., and
- 652 Papadopol, P.: Development and Testing of Canada-Wide Interpolated Spatial Models of Daily Minimum–





- Maximum Temperature and Precipitation for 1961–2003, *Journal of Applied Meteorology and Climatology*, 48, 725–741, 10.1175/2008jamc1979.1, 2009.
- IPCC: Climate Change 2013: The Physical Science Basis. Contribution of Working Group I to the Fifth Assessment Report of the Intergovernmental Panel on Climate Change, Cambridge University Press, Cambridge, United Kingdom and New York, NY, USA, 1535 pp., 2013.
- Jiang, R., Gan, T. Y., Xie, J., and Wang, N.: Spatiotemporal variability of Alberta's seasonal precipitation, their teleconnection with large-scale climate anomalies and sea surface temperature, *International Journal of Climatology*, 34, 2899–2917, 10.1002/joc.3883, 2014.
- Mantua, N. J., and Hare, S. R.: The Pacific Decadal Oscillation, *Journal of Oceanography*, 58, 35–44, 10.1023/a:1015820616384, 2002.
- Masud, M. B., Khaliq, M. N., and Wheeler, H. S.: Analysis of meteorological droughts for the Saskatchewan River Basin using univariate and bivariate approaches, *Journal of Hydrology*, 522, 452–466, <http://dx.doi.org/10.1016/j.jhydrol.2014.12.058>, 2015.
- Masud, M. B., Khaliq, M. N., and Wheeler, H. S.: Future changes to drought characteristics over the Canadian Prairie Provinces based on NARCCAP multi-RCM ensemble, *Climate Dynamics*, 48, 2685–2705, 10.1007/s00382-016-3232-2, 2017.
- McKee, T., Doesken, N., and Kleist, J.: The Relationship of Drought Frequency and Duration to Time Scales. Paper Presented at 8th Conference on Applied Climatology. American Meteorological Society: Anaheim, CA., 1993.
- McKenney, D. W., Hutchinson, M. F., Papadopol, P., Lawrence, K., Pedlar, J., Campbell, K., Milewska, E., Hopkinson, R. F., Price, D., and Owen, T.: Customized Spatial Climate Models for North America, *Bulletin of the American Meteorological Society*, 92, 1611–1622, 10.1175/2011bams3132.1, 2011.
- Mekis, É., and Vincent, L. A.: An Overview of the Second Generation Adjusted Daily Precipitation Dataset for Trend Analysis in Canada, *Atmosphere-Ocean*, 49, 163–177, 10.1080/07055900.2011.583910, 2011.
- Mishra, A. K., and Singh, V. P.: A review of drought concepts, *Journal of Hydrology*, 391, 202–216, <http://dx.doi.org/10.1016/j.jhydrol.2010.07.012>, 2010.
- Mishra, A. K., and Singh, V. P.: Drought modeling – A review, *Journal of Hydrology*, 403, 157–175, <http://dx.doi.org/10.1016/j.jhydrol.2011.03.049>, 2011.
- Nazemi, A., Wheeler, H. S., Chun, K. P., Bonsal, B., and Mekonnen, M.: Forms and drivers of annual streamflow variability in the headwaters of Canadian Prairies during the 20th century, *Hydrological Processes*, 31, 221–239, 10.1002/hyp.11036, 2017.
- Ng, E. K., and Chan, J. C.: Geophysical applications of partial wavelet coherence and multiple wavelet coherence, *Journal of Atmospheric and Oceanic Technology*, 29, 1845–1853, 2012.
- North, G. R., Bell, T. L., Cahalan, R. F., and Moeng, F. J.: Sampling Errors in the Estimation of Empirical Orthogonal Functions, *Monthly Weather Review*, 110, 699–706, 10.1175/1520-0493(1982)110<0699:seiteo>2.0.co;2, 1982.
- Palmer, W.: Meteorological drought, Research Paper No. 45. U.S. Weather Bureau. (NOAA Library and Information Services Division, Washington, D.C. 20852), 1–25., 1965.
- Penman, H. L.: Natural evaporation from open water, bare soil and grass, *Proceedings of the Royal Society of London. Series A. Mathematical and Physical Sciences*, 193, 120–145, 10.1098/rspa.1948.0037, 1948.
- Perez-Valdivia, C., Sauchyn, D., and Vanstone, J.: Groundwater levels and teleconnection patterns in the Canadian Prairies, *Water Resources Research*, 48, n/a–n/a, 10.1029/2011WR010930, 2012.
- Perez-Valdivia, C., Sauchyn, D., and Vanstone, J.: Groundwater levels and teleconnection patterns in the Canadian Prairies, *Water Resources Research*, 48, 2012.
- Pomeroy, J. W., Fang, X., and Marks, D. G.: The cold rain-on-snow event of June 2013 in the Canadian Rockies — characteristics and diagnosis, *Hydrological Processes*, 30, 2899–2914, 10.1002/hyp.10905, 2016.
- Preisendorfer, R. W., and Mobley, C. D.: Principal component analysis in meteorology and oceanography, Elsevier Amsterdam, 1988.



- Priestley, C. H. B., and Taylor, R. J.: On the Assessment of Surface Heat Flux and Evaporation Using Large-Scale Parameters, *Monthly Weather Review*, 100, 81-92, 10.1175/1520-0493(1972)100<0081:otaosh>2.3.co;2, 1972.
- Raible, C. C., Bärend, O., and Gómez-navarro, J. J.: Drought indices revisited – improving and testing of drought indices in a simulation of the last two millennia for Europe, *Tellus A: Dynamic Meteorology and Oceanography*, 69, 1287492, 10.1080/16000870.2017.1296226, 2017.
- Razavi, S., and Vogel, R.: Prewhitening of hydroclimatic time series? Implications for inferred change and variability across time scales, *Journal of Hydrology*, 557, 109-115, <https://doi.org/10.1016/j.jhydrol.2017.11.053>, 2018.
- Richman, M. B.: Rotation of principal components, *Journal of Climatology*, 6, 293-335, 10.1002/joc.3370060305, 1986.
- Ropelewski, C. F., and Halpert, M. S.: North American Precipitation and Temperature Patterns Associated with the El Niño/Southern Oscillation (ENSO), *Monthly Weather Review*, 114, 2352-2362, 10.1175/1520-0493(1986)114<2352:napatp>2.0.co;2, 1986.
- Shabbar, A., and Khandekar, M.: The impact of el Nino-Southern oscillation on the temperature field over Canada: Research note, *Atmosphere-Ocean*, 34, 401-416, 10.1080/07055900.1996.9649570, 1996.
- Shabbar, A., and Skinner, W.: Summer Drought Patterns in Canada and the Relationship to Global Sea Surface Temperatures, *Journal of Climate*, 17, 2866-2880, 10.1175/1520-0442(2004)017<2866:sdpica>2.0.co;2, 2004.
- Shabbar, A., and Yu, B.: Intraseasonal Canadian Winter Temperature Responses to Interannual and Interdecadal Pacific SST Modulations, *Atmosphere-Ocean*, 50, 109-121, 10.1080/07055900.2012.657154, 2012.
- Sheffield, J., Andreadis, K. M., Wood, E. F., and Lettenmaier, D. P.: Global and Continental Drought in the Second Half of the Twentieth Century: Severity–Area–Duration Analysis and Temporal Variability of Large-Scale Events, *Journal of Climate*, 22, 1962-1981, 10.1175/2008jcli2722.1, 2009.
- Sheridan, S. C.: North American weather-type frequency and teleconnection indices, *International journal of climatology*, 23, 27-45, 2003.
- Sternberg, T.: Regional drought has a global impact, *Nature*, 472, 169-169, 2011.
- Szeto, K., Zhang, X., White, R. E., and Brimelow, J.: The 2015 Extreme Drought in Western Canada, *Bulletin of the American Meteorological Society*, 97, S42-S46, 10.1175/bams-d-16-0147.1, 2016.
- Tallaksen, L. M., and Stahl, K.: Spatial and temporal patterns of large-scale droughts in Europe: Model dispersion and performance, *Geophysical Research Letters*, 41, 429-434, 10.1002/2013GL058573, 2014.
- Thornthwaite, C. W.: An Approach toward a Rational Classification of Climate, *Geographical Review*, 38, 55-94, 10.2307/210739, 1948.
- Torrence, C., and Compo, G. P.: A Practical Guide to Wavelet Analysis, *Bulletin of the American Meteorological Society*, 79, 61-78, 10.1175/1520-0477(1998)079<0061:apgtwa>2.0.co;2, 1998.
- Torrence, C., and Webster, P. J.: Interdecadal Changes in the ENSO–Monsoon System, *Journal of Climate*, 12, 2679-2690, 10.1175/1520-0442(1999)012<2679:icitem>2.0.co;2, 1999.
- Tremblay, L., Larocque, M., Anctil, F., and Rivard, C.: Teleconnections and interannual variability in Canadian groundwater levels, *Journal of Hydrology*, 410, 178-188, 2011.
- Uvo, C. B.: Analysis and regionalization of northern European winter precipitation based on its relationship with the North Atlantic oscillation, *International Journal of Climatology*, 23, 1185-1194, 10.1002/joc.930, 2003.
- Van Loon, A. F., Stahl, K., Di Baldassarre, G., Clark, J., Rangecroft, S., Wanders, N., Gleeson, T., Van Dijk, A. I., Tallaksen, L. M., and Hannaford, J.: Drought in a human-modified world: reframing drought definitions, understanding, and analysis approaches, *Hydrology and Earth System Sciences*, 20, 3631, 2016.
- Vicente-Serrano, S. M., Beguería, S., and López-Moreno, J. I.: A Multiscalar Drought Index Sensitive to Global Warming: The Standardized Precipitation Evapotranspiration Index, *Journal of Climate*, 23, 1696-1718, 10.1175/2009jcli2909.1, 2010.



- 751 Vincent, L. A., Wang, X. L., Milewska, E. J., Wan, H., Yang, F., and Swail, V.: A second generation of  
752 homogenized Canadian monthly surface air temperature for climate trend analysis, *Journal of Geophysical*  
753 *Research: Atmospheres*, 117, n/a-n/a, 10.1029/2012JD017859, 2012.
- 754 Vincent, L. A., Zhang, X., Brown, R. D., Feng, Y., Mekis, E., Milewska, E. J., Wan, H., and Wang, X. L.:  
755 Observed Trends in Canada's Climate and Influence of Low-Frequency Variability Modes, *Journal of*  
756 *Climate*, 28, 4545-4560, 10.1175/jcli-d-14-00697.1, 2015.
- 757 Wang, X. L., and Lin, A.: An algorithm for integrating satellite precipitation estimates with in situ  
758 precipitation data on a pentad time scale, *Journal of Geophysical Research: Atmospheres*, 120, 3728-3744,  
759 10.1002/2014JD022788, 2015.
- 760 Wells, N., Goddard, S., and Hayes, M. J.: A Self-Calibrating Palmer Drought Severity Index, *Journal of*  
761 *Climate*, 17, 2335-2351, 10.1175/1520-0442(2004)017<2335:aspdsi>2.0.co;2, 2004.
- 762 Wheeler, H., and Gober, P.: Water security in the Canadian Prairies: science and management challenges,  
763 *Philosophical Transactions of the Royal Society A: Mathematical,*  
764 *Physical and Engineering Sciences*, 371, 10.1098/rsta.2012.0409, 2013.
- 765 Wheeler, H., and Gober, P.: Water security and the science agenda, *Water Resources Research*, 51, 5406-  
766 5424, 10.1002/2015WR016892, 2015.
- 767 Wheaton, E., Arthur, L., Chorney, B., Shewchuk, S., Thorpe, J., Whiting, J., and Wittrock, V.: The prairie  
768 drought of 1988, *Climatological Bulletin*, 26, 188-205, 1992.
- 769 Wilhite, D. A., and Glantz, M. H.: Understanding: the Drought Phenomenon: The Role of Definitions,  
770 *Water International*, 10, 111-120, 10.1080/02508068508686328, 1985.
- 771 Wilhite, D. A.: Drought as a natural hazard: Concepts and definitions. *Drought: A Global Assessment*, 3–  
772 18, 2000a.
- 773 Wilhite, D. A.: Drought as a natural hazard: concepts and definitions, 2000b.
- 774 Wilks, D. S.: Statistical methods in the atmospheric sciences, Academic press, 2011.
- 775 Wolter, K.: The Southern Oscillation in Surface Circulation and Climate over the Tropical Atlantic, Eastern  
776 Pacific, and Indian Oceans as Captured by Cluster Analysis, *Journal of Climate and Applied Meteorology*,  
777 26, 540-558, 10.1175/1520-0450(1987)026<0540:tsoisc>2.0.co;2, 1987.
- 778 Wolter, K., and Timlin, M. S.: El Niño/Southern Oscillation behaviour since 1871 as diagnosed in an  
779 extended multivariate ENSO index (MEI.ext), *International Journal of Climatology*, 31, 1074-1087,  
780 10.1002/joc.2336, 2011.
- 781 Wong, J. S., Razavi, S., Bonsal, B. R., Wheeler, H. S., and Asong, Z. E.: Evaluation of various daily  
782 precipitation products for large-scale hydro-climatic applications over Canada, *Hydrol. Earth Syst. Sci.*  
783 *Discuss.*, 2016, 1-51, 10.5194/hess-2016-511, 2016.
- 784 Yue, S., Pilon, P., Phinney, B., and Cavadias, G.: The influence of autocorrelation on the ability to detect  
785 trend in hydrological series, *Hydrological processes*, 16, 1807-1829, 2002.
- 786 Zhang, X., Vincent, L. A., Hogg, W. D., and Niitsoo, A.: Temperature and precipitation trends in Canada  
787 during the 20th century, *Atmosphere-Ocean*, 38, 395-429, 10.1080/07055900.2000.9649654, 2000.
- 788 Zhang, X., Harvey, K. D., Hogg, W. D., and Yuzyk, T. R.: Trends in Canadian streamflow, *Water Resources*  
789 *Research*, 37, 987-998, 10.1029/2000WR900357, 2001.
- 790 Zhao, H., Higuchi, K., Waller, J., Auld, H., and Mote, T.: The impacts of the PNA and NAO on annual  
791 maximum snowpack over southern Canada during 1979–2009, *International Journal of Climatology*, 33,  
792 388-395, 10.1002/joc.3431, 2013.
- 793 Zhou, S., Miller, A. J., Wang, J., and Angell, J. K.: Trends of NAO and AO and their associations with  
794 stratospheric processes, *Geophysical Research Letters*, 28, 4107-4110, 10.1029/2001GL013660, 2001.

795

796



797 **List of Tables**

798 **Table 1:** Categories of dryness/wetness degree according to the SPEI values (McKee et al., 1993)

Categories	SPEI classifications
Extremely dry	$\leq -2.00$
Severely dry	$-1.99$ to $-1.50$
Moderately dry	$-1.49$ to $-1.00$
Near normal	$-0.99$ to $0.99$
Moderately wet	$1.00$ to $1.49$
Severely wet	$1.50$ to $1.99$
Extremely wet	$\geq 2.00$

799

800 **Table 2:** Percentage of grids with decreasing (Dec.) and increasing (Inc.) trends for the SPEI

	ANUSPLIN		CANGRD	
	Inc.	Dec.	Inc.	Dec.
<b>SPEI1</b>	8.9	14.7	8.6	5.9
<b>SPEI3</b>	4.1	10.6	5.4	3.0
<b>SPEI6</b>	2.8	9.6	3.7	2.3
<b>SPEI12</b>	1.4	10.0	2.9	4.0
<b>SPEI<sub>APR-SEPT</sub></b>	0.9	6.2	2.2	4.0
<b>SPEI<sub>OCT-SEPT</sub></b>	1.2	10.0	2.7	3.1

801

802 **Table 3:** Percentage of variance explained by the first two varimax rotated loadings (REOFs) of the SPEI

803 at various time scales computed using observations from ANUSPLIN and CANGRD data sets

	ANUSPLIN		CANGRD	
	REOF1	REOF2	REOF1	REOF2
<b>SPEI1</b>	15.0	13.2	19.5	11.9
<b>SPEI3</b>	15.8	13.8	18.9	12.9
<b>SPEI6</b>	17.9	14.4	19.1	12.7
<b>SPEI12</b>	20.6	13.3	19.1	13.0
<b>SPEI<sub>APR-SEPT</sub></b>	19.5	12.6	16.5	11.7
<b>SPEI<sub>OCT-SEPT</sub></b>	20.5	13.4	19.3	13.1

804

805

806

807



**Table 4:** Long-term (1950–2013) trends of monthly time series (RPCs) for the first two REOFs of SPEI at various time scales. The slope year<sup>-1</sup> (a) and *p*-value (b) is indicated, with significant ( $p < 0.05$ ) trends shown in bold.

	ANUSPLIN				CANGRD			
	REOF1		REOF2		REOF1		REOF2	
	(a)	(b)	(a)	(b)	(a)	(b)	(a)	(b)
<b>SPEI3</b>	1.3e-04	0.432	1.6e-04	0.334	1.3e-04	0.410	-1.0e-04	0.539
<b>SPEI6</b>	-2.3e-04	0.157	-1.3e-05	0.935	-4.5e-05	0.787	-5.1e-04	<b>0.002</b>
<b>SPEI12</b>	-1.8e-05	0.909	5.4e-04	<b>0.001</b>	2.6e-05	0.873	6.4e-04	<b>1.0e-04</b>
<b>SPEI6<sub>Apr-Sept</sub></b>	-8.5e-05	0.855	-3.2e-04	0.492	-1.7e-03	<b>1.0e-04</b>	1.0e-03	<b>0.026</b>
<b>SPEI12<sub>Oct-Sept</sub></b>	-1.2e-04	0.456	-3.7e-04	<b>0.029</b>	-4.6e-05	0.785	-4.6e-04	<b>0.006</b>

**Table 5:** Dominant periods and the intervals of significant variance for SPEI6<sub>Apr-Sept</sub> and SPEI12<sub>Oct-Sept</sub> during 1950–2013.

	Dominant periods		Intervals of variance
	REOF1 (Prairie)	8 – 32	1955 – 2001; 2002 – 2013
<b>SPEI6<sub>Apr-</sub></b>	REOF2 (Northern)	8 – 40	1955 – 2000
<b>SPEI12<sub>Oct-</sub></b>	REOF1 (Prairie)	16 – 60; 32 – 64	1955 – 1968; 1970 – 2002
	REOF2 (Northern)	16 – 100	1956 – 1975; 1995 – 2013



823 **Figure captions**

824 **Figure 1.** Study area showing topographic and hydrographic features of Canada.

825 **Figure 2.** Mean annual climatology of precipitation, minimum ( $T_{min}$ ) and maximum ( $T_{max}$ ) temperature  
 826 for the period 1950 – 2013.

827 **Figure 3.** Spatial structure of long-term mean monthly water surplus/deficit (mm), i.e.  $P-PET$ , derived from  
 828 ANUSPLIN (a) and CANGRD (b).

829 **Figure 4.** Trends in SPEI at each grid point for ANUSPLIN and CANGRD. Only significant values are  
 830 shown on the map. Brown indicates decreasing and green is increasing. **a**=SPEI at 1 month, **b**=SPEI at 3  
 831 months, **c**=SPEI at 6 months, **d**=SPEI at 12 months, **e**=SPEI at 6 months from April –Sept, **f**=SPEI at  
 832 12months of the water/hydrologic year i.e. Oct – Sept. Trends are significant at 95% confidence level.

833 **Figure 5.** Spatial patterns of the first two REOFs of SPEI at various time scales. The spatial extent of the  
 834 first two REOFs was characterized by mapping the values of the factorial matrix. See Table 3 for  
 835 information on variances explained by each REOF pattern.

836 **Figure 6.** Temporal patterns (RPCs) of the first two rotated principal components (REOFs) of SPEI at  
 837 various time scales. Indicated within each box is the pattern correlation between ANUSPLIN and  
 838 CANGRD.

839 **Figure 7.** Long-term (1950–2013) trends (red line) of the RPCs for each drought sub-region and data set.

840 **Figure 8.** Wavelet power spectrum of the time series (RPCs) shown in Fig. 6. The black contour designates  
 841 the 95% confidence level against red noise, and the cone of the influence (COI) where edge effects might  
 842 distort the picture is shown as a lighter grey shade.

843 **Figure 9.** Squared wavelet coherence between the MEI and the temporal patterns of drought ( $SPEI6_{Apr\_Sept}$   
 844 and  $SPEI12_{Oct\_Sept}$ ). Phase arrows pointing right indicate signals are in phase, whereas a left-pointing arrows  
 845 indicate an antiphase relationship. Arrows deviating from the horizontal are indicative of lead-lag  
 846 relationships between the two signals. The black contour designates the 95% confidence level against red  
 847 noise, and the cone of the influence (COI) where edge effects might distort the picture is shown as a lighter  
 848 grey shade.



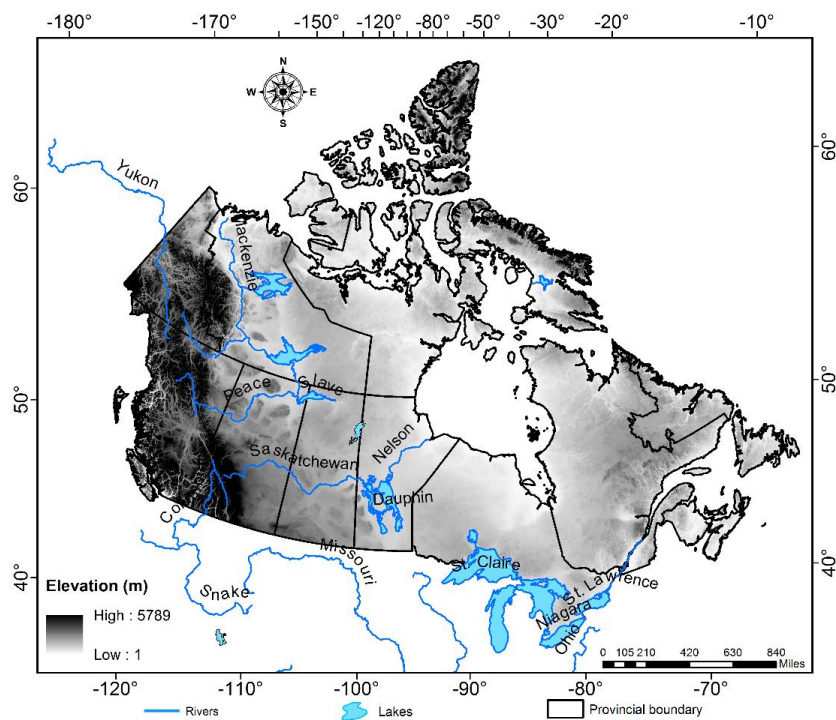
849 **Figure 10.** Squared wavelet coherence between the PDO and the temporal patterns of drought (SPEI6<sub>Apr\_Sept</sub>  
850 and SPEI12<sub>Oct\_Sept</sub>). Phase arrows pointing right indicate signals are in phase, whereas a left-pointing arrows  
851 indicate an antiphase relationship. Arrows deviating from the horizontal are indicative of lead-lag  
852 relationships between the two signals. The black contour designates the 95% confidence level against red  
853 noise, and the cone of the influence (COI) where edge effects might distort the picture is shown as a lighter  
854 grey shade.

855 **Figure 11.** Squared wavelet coherence between the PNA and the temporal patterns of drought (SPEI6<sub>Apr\_Sept</sub>  
856 and SPEI12<sub>Oct\_Sept</sub>). Phase arrows pointing right indicate signals are in phase, whereas a left-pointing arrows  
857 indicate an antiphase relationship. Arrows deviating from the horizontal are indicative of lead-lag  
858 relationships between the two signals. The black contour designates the 95% confidence level against red  
859 noise, and the cone of the influence (COI) where edge effects might distort the picture is shown as a lighter  
860 grey shade.





## 861 List of Figures

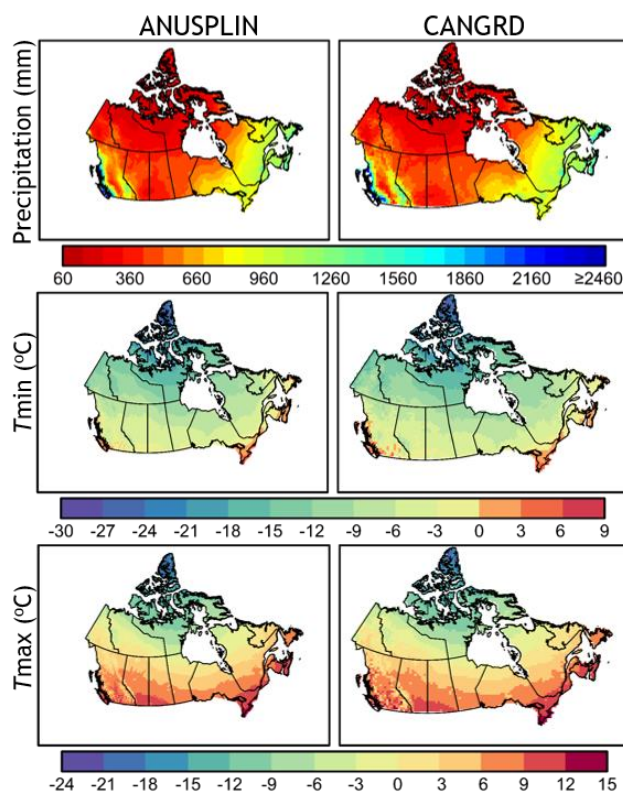


862  
 863 **Figure 1.** Study area showing topographic and hydrographic features of Canada.

864

865



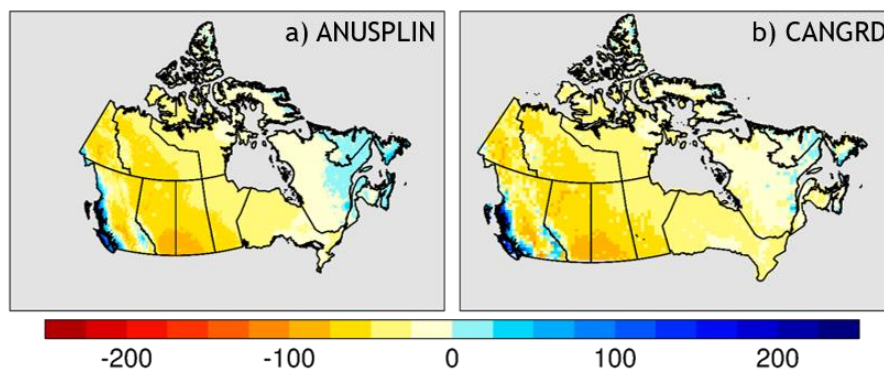


866

867 **Figure 2.** Mean annual climatology of precipitation, minimum ( $T_{min}$ ) and maximum ( $T_{max}$ ) temperature  
 868 for the period 1950 – 2013.

869

870



871

872 **Figure 3.** Spatial structure of long-term mean monthly water surplus/deficit (mm), i.e.  $P$ -PET, derived from  
 873 ANUSPLIN (a) and CANGRD (b).

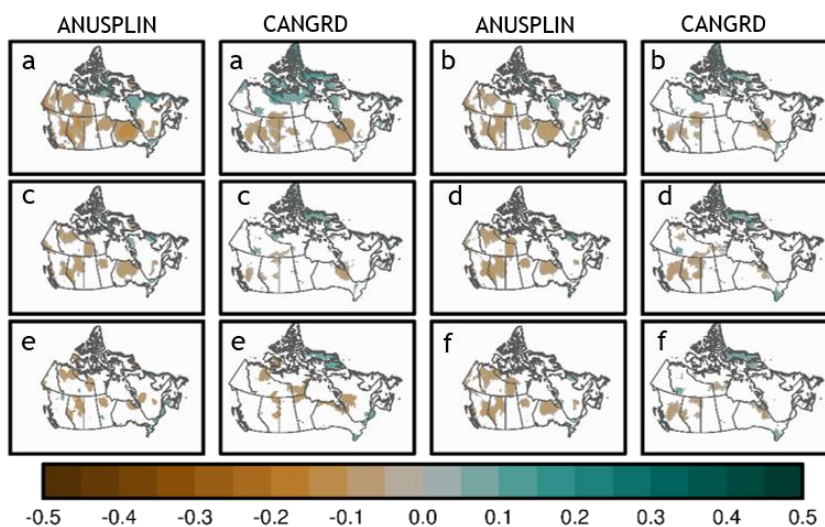
874

875

876

877

878



879

880 **Figure 4.** Trends in SPEI at each grid point for ANUSPLIN and CANGRD. Only significant values are  
 881 shown on the map. Brown indicates decreasing and green is increasing. **a**=SPEI at 1 month, **b**=SPEI at 3  
 882 months, **c**=SPEI at 6 months, **d**=SPEI at 12 months, **e**=SPEI at 6 months from April –Sept, **f**=SPEI at  
 883 12months of the water/hydrologic year i.e. Oct – Sept. Trends are significant at 95% confidence level.

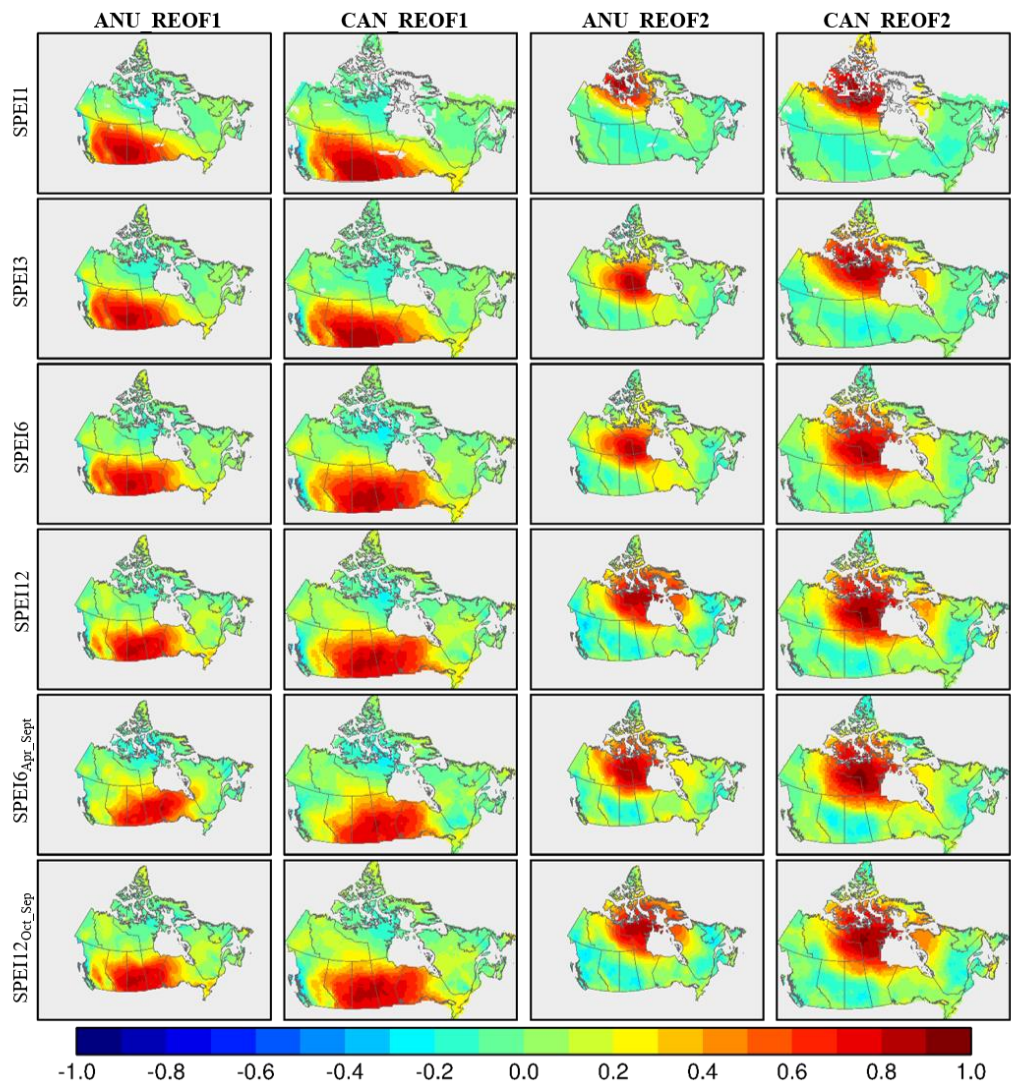
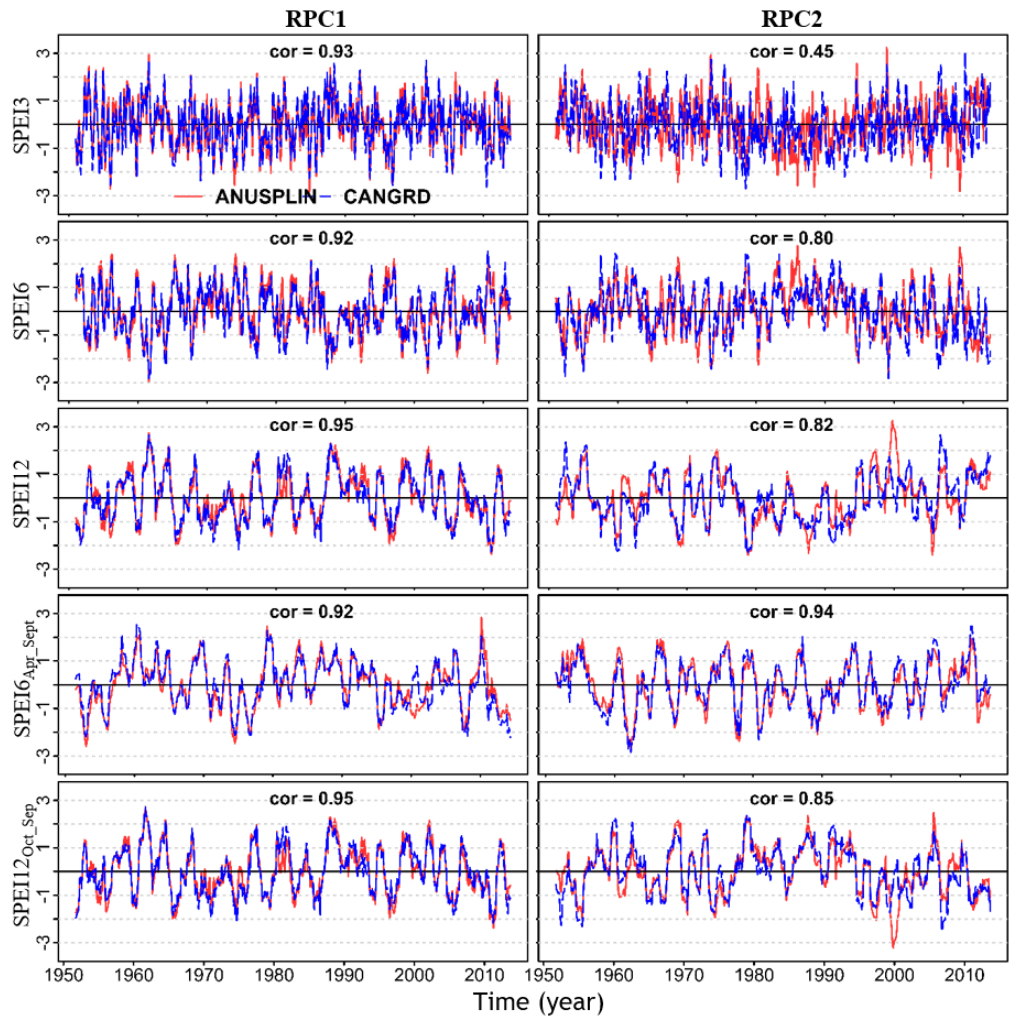


**Figure 5.** Spatial patterns of the first two REOFs of SPEI at various time scales. The spatial extent of the first two REOFs was characterized by mapping the values of the factorial matrix. See Table 3 for information on variances explained by each REOF pattern.



888

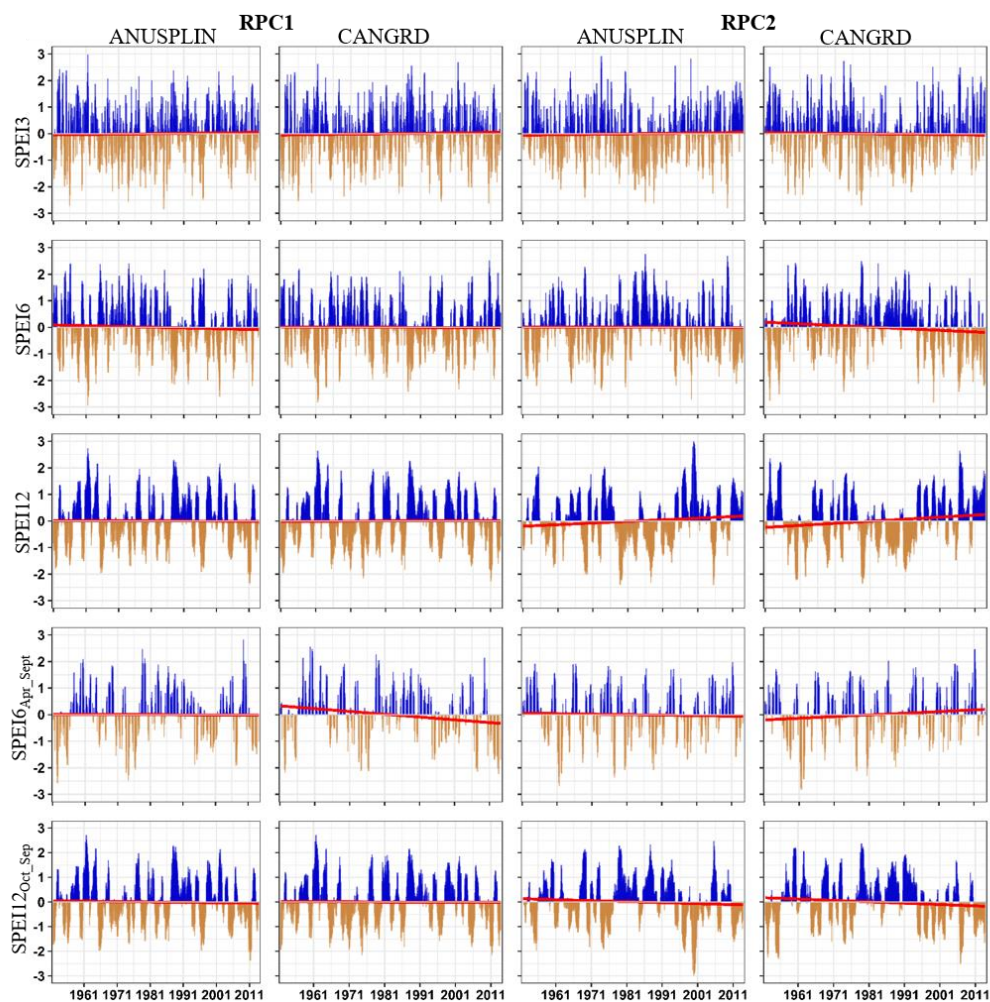
889 **Figure 6.** Temporal patterns (RPCs) of the first two rotated principal components (REOFs) of SPEI at  
890 various time scales. Indicated within each box is the pattern correlation between ANUSPLIN and  
891 CANGRD.

892

893

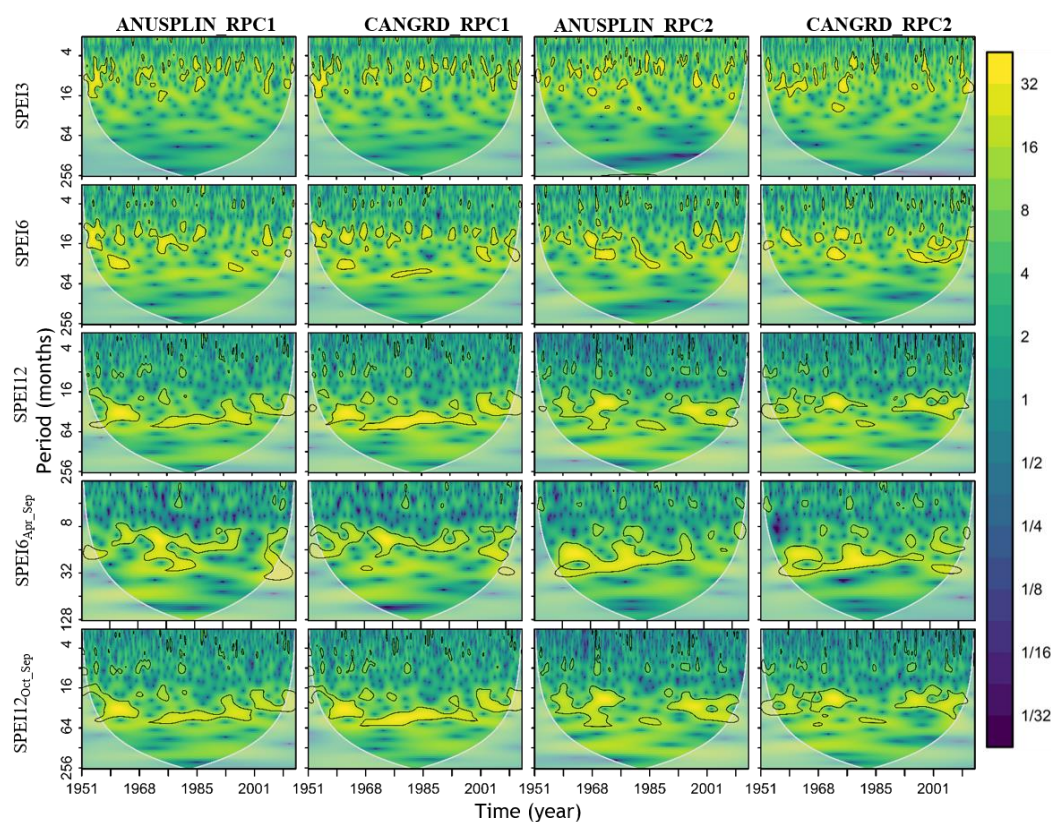
894





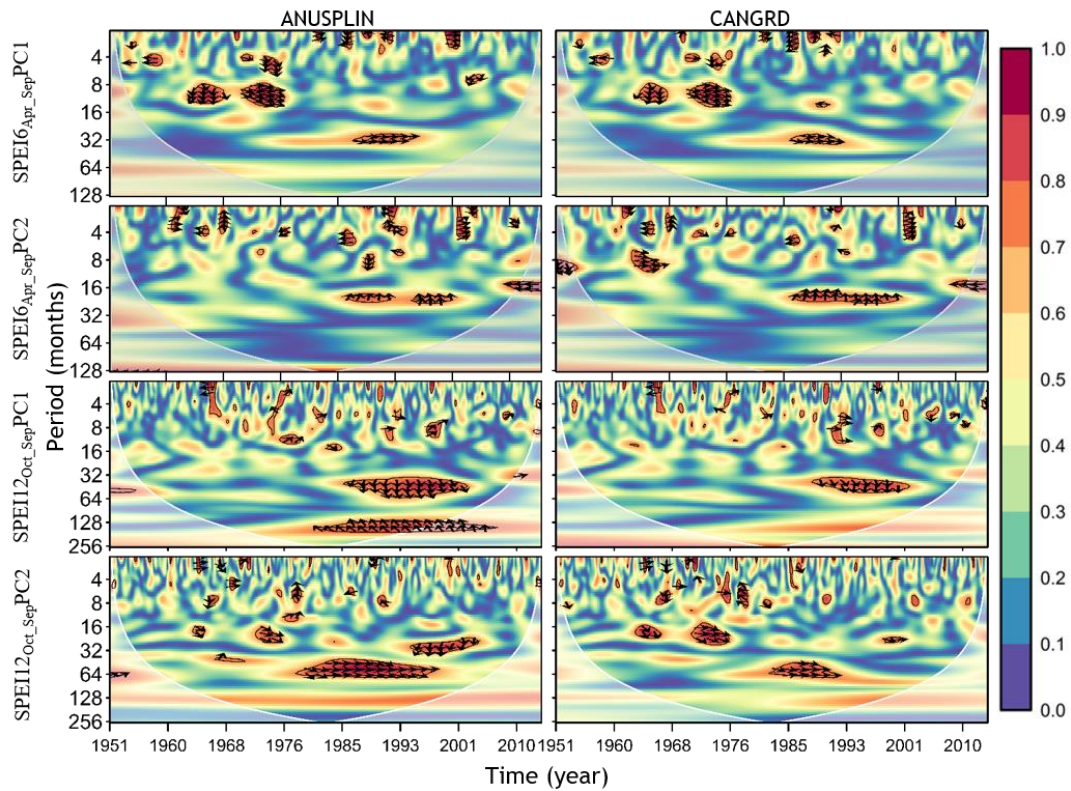
895

896 **Figure 7.** Long-term (1950–2013) trends (red line) of the RPCs for each drought sub-region and data set.



897

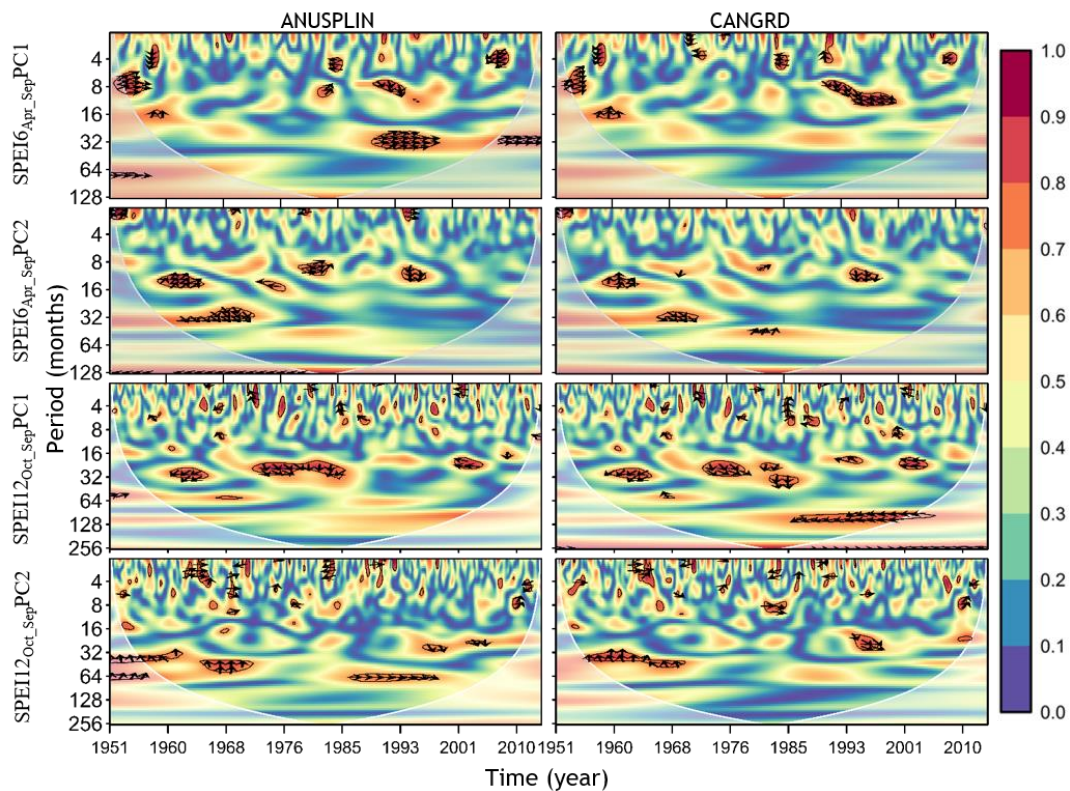
898 **Figure 8.** Wavelet power spectrum of the time series (RPCs) shown in Fig. 6. The black contour designates  
 899 the 95% confidence level against red noise, and the cone of the influence (COI) where edge effects might  
 900 distort the picture is shown as a lighter grey shade.



901

902 **Figure 9.** Squared wavelet coherence between the MEI and the temporal patterns of drought (SPEI6<sub>Apr\_Sept</sub>  
903 and SPEI12<sub>Oct\_Sept</sub>). Phase arrows pointing right indicate signals are in phase, whereas a left-pointing arrows  
904 indicate an antiphase relationship. Arrows deviating from the horizontal are indicative of lead-lag  
905 relationships between the two signals. The black contour designates the 95% confidence level against red  
906 noise, and the cone of the influence (COI) where edge effects might distort the picture is shown as a lighter  
907 grey shade.





908

909 **Figure 10.** Squared wavelet coherence between the PDO and the temporal patterns of drought (SPEI6<sub>Apr\_Sep</sub>  
910 and SPEI12<sub>Oct\_Sept</sub>). Phase arrows pointing right indicate signals are in phase, whereas a left-pointing arrows  
911 indicate an antiphase relationship. Arrows deviating from the horizontal are indicative of lead-lag  
912 relationships between the two signals. The black contour designates the 95% confidence level against red  
913 noise, and the cone of the influence (COI) where edge effects might distort the picture is shown as a lighter  
914 grey shade.

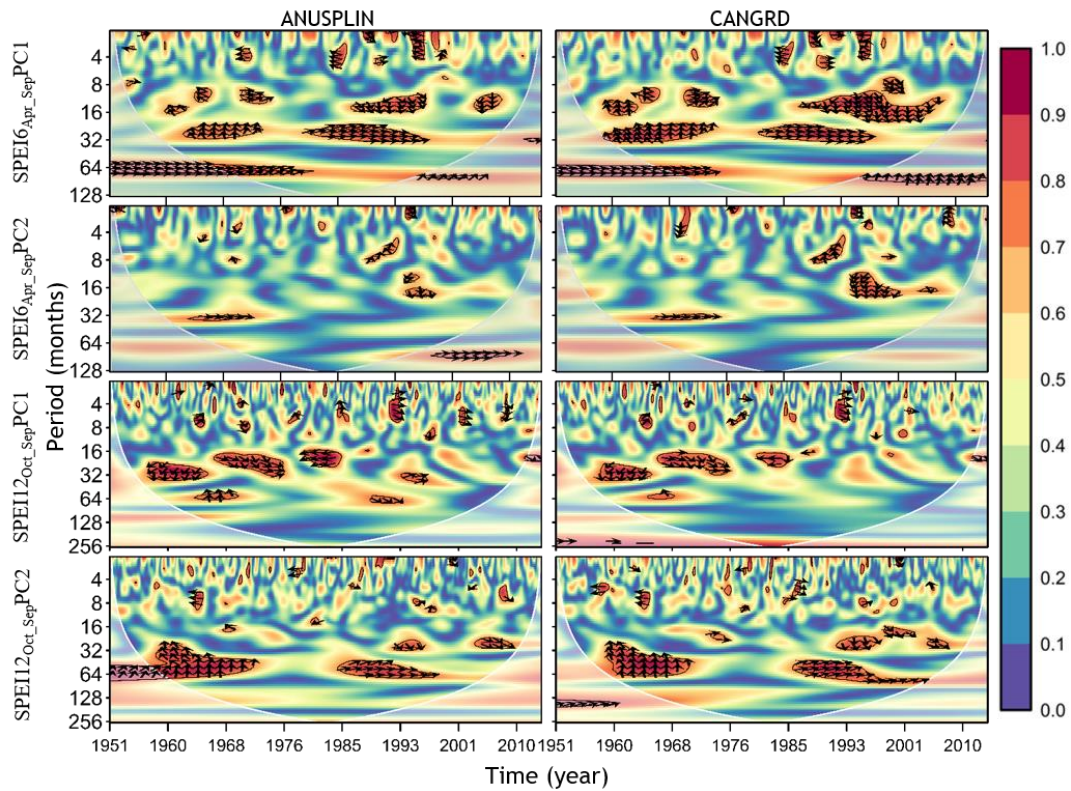


**Figure 11.** Squared wavelet coherence between the PNA and the temporal patterns of drought (SPEI6<sub>Apr\_Sept</sub> and SPEI12<sub>Oct\_Sept</sub>). Phase arrows pointing right indicate signals are in phase, whereas a left-pointing arrows indicate an antiphase relationship. Arrows deviating from the horizontal are indicative of lead-lag relationships between the two signals. The black contour designates the 95% confidence level against red noise, and the cone of the influence (COI) where edge effects might distort the picture is shown as a lighter grey shade.